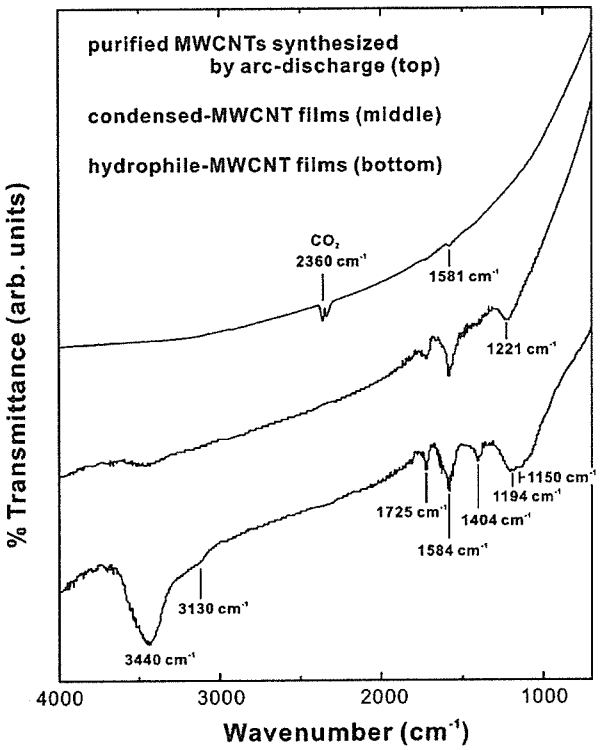

Figure 2. FT-IR spectra of purified MWCNTs synthesized by arc-discharge method (top), condensed-MWCNT films (middle), and hydrophile-MWCNT films (bottom).

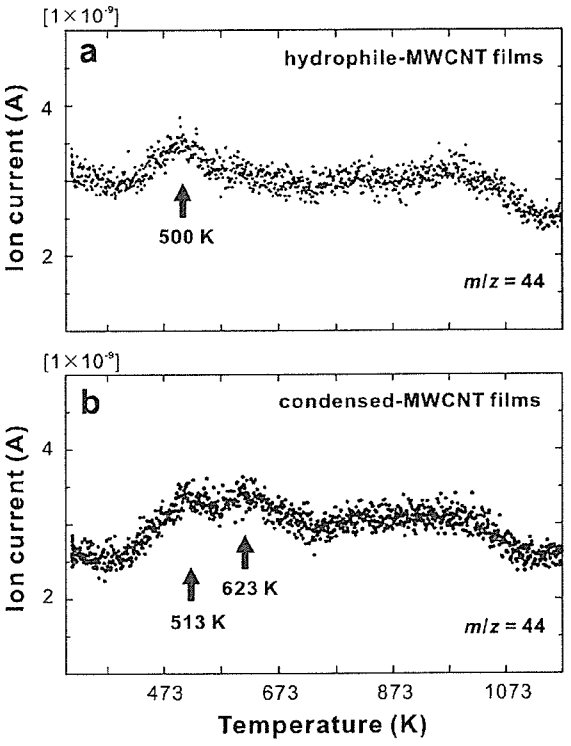

Figure 3. Generation of CO_2 (m/z 44) of (a) hydrophile-MWCNT and (b) condensed-MWCNT films in a helium atmosphere.

hand, the I_D/I_G of hydrophile-MWCNT films and condensed-MWCNT films was approximately 1.07 and 1.08, respectively, and is greater than that of purified-MWCNTs. This indicates that both hydrophile- and condensed-MWCNT films possess covalent functionalization, and the number of functionalized covalent bonds to the nanotube is very similar.

The degree of functionalization has been determined by TG-Mass from 303 to 1173 K under a helium gas flow. As water in the samples was vaporized in vacuo (10^{-3} Torr) at 333 K for over 12 h prior to TG-mass analysis, water molecules were not observed. The generation of CO_2 (m/z 44) was confirmed around 473 K and between 773 and 1073 K for both samples (Figure 3). According to other studies on activated carbon[17] and carbon nanofibers[15] with oxygen surface groups, the maxima on the CO_2 profile are due to the decomposition of carboxylic groups. In the same way, the generation of CO_2 from the nanotube films is attributed to the decomposition of carboxylic acid, ester, lactones, and carbonyl groups under a helium gas flow at less than 1073 K. In the range from 473 to 673 K, the amount of CO_2 gas generated from hydrophile-MWCNT films was marked at 500 K (Figure 3a). On the other hand, the amount of CO_2 gas generated from condensed-MWCNT films was marked at 515 and 623 K (Figure 3b). Condensed-MWCNT films showed a new CO_2-generating maximum at 623 K, in sharp contrast to that of hydrophile-MWCNT films, which might be due to the decomposition of ester bonds. We consider that the difference in temperature associated with the generated CO_2 is dependent on the functional groups (here, ester groups) and the nanotube surface site (end or body of the nanotube) that the functional groups are bonded to, and where the decomposition energy of carboxylic groups and derivatives into CO_2 differs. Although CO gas was confirmed between 573 and 1073 K for both samples, the generated CO gas was very low. According to studies of surface oxidation on fishbone-type carbon nanofibers,[15] the generated CO gas was very high around 873 K using TGA-mass analysis, and the evolution of CO is attributed to the decomposition of quinones, hydroquinones, and phenols. The reason the generated CO gas is low in our samples is due to the geometry of graphene structure. In fishbone- or herringbone-type carbon nanofibers, as the graphitic planes are oriented at an angle to the fiber axis,[18] the surface oxidation of groups such as phenol and quinones abundantly occurs at the edges of the graphitic planes in comparison to the basal plane of the graphene of carbon nanotubes. Given the aforementioned results, it was determined that functional groups such as carboxylic acids and esters decompose into CO_2 by ca. 1173 K.

The typical weight loss for the hydrophile-MWCNT films and condensed-MWCNT films up to 1173 K was approximately 12.2 and 11.5 wt %, respectively (Figure 4). As water is produced by the dehydration−condensation reaction, the difference in weight loss percentage of both films is represented by the ratio of water produced. As the difference in weight loss percentage between hydrophile-MWCNT and condensed-MWCNT films by 1173 K is essentially a weight percentage of the water molecules generated, the molar (X) of the water molecules generated is as follows:

$$X = [(W_h - W_{cond})M_{total}]/1800 \text{ (mol)}$$

Here, W_h is 12.2 wt % of weight loss percentage for the hydrophile-MWCNT films at 1173 K and W_{cond} is 11.5 wt % of weight loss percentage for the condensed-MWCNT films at 1173 K. M_{total} is the total weight of the films. As the apparent density of both samples is 0.59 g/cm^3, the molar amount of the water molecules generated per unit apparent volume (cm^3) of MWCNT films is 2.29×10^{-4} mol/cm^3. Assuming that ester bonds are uniformly formed all over the condensed-MWCNT films, as a water molecule is produced and an ester bond is

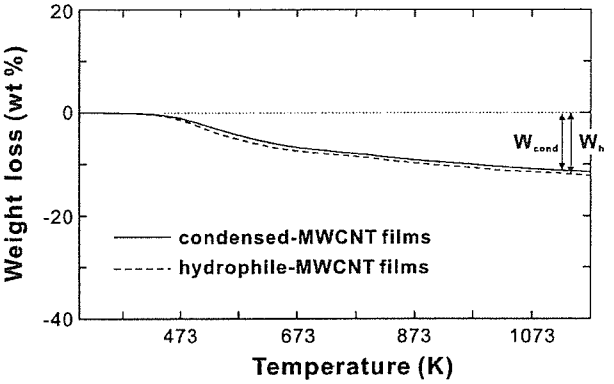

Figure 4. TG curves of hydrophile-MWCNT (dashed line) and condensed-MWCNT (solid line) films. W_h and W_{cond} represent the decreasing weight percentage of hydrophile-MWCNT and condensed-MWCNT films, respectively, at 1173 K.

formed, the number of ester cross-links formed per unit apparent volume of condensed-MWCNT films is 1.37×10^{20} bonds/cm^3. In the same way, the molar amount (Y) of the carbon of the nanotubes per unit apparent volume of MWCNT films is as follow:

$$Y = [(W'_{cond} - W_{metal})M_{total}]/1200 \text{ (mol)}$$

Here, W'_{cond} is 88.5 wt % of the weight percentage ($100 - W_{cond}$) for the condensed-MWCNT films from which the functional groups decomposed following condensation, and W_{metal} is 0.5 wt % of the weight percentage of metal in the condensed-MWCNT films. M_{total} is the total weight of the films. When the apparent density of the condensed-MWCNT films is 0.59 g/cm^3, the molar amount of the carbon of the nanotubes per unit apparent volume of MWCNT films is 4.32×10^{-2} mol/cm^3. The number of carbon atoms of the nanotubes per unit apparent volume of condensed-MWCNT films is 2.60×10^{22} carbon atoms/cm^3. Consequently, the ratio (cross-link$_{ester}$/$C_{nanotube}$) of the number of ester cross-links and carbon atoms of the nanotubes per unit apparent volume (cm^3) of MWCNT films is 5.27×10^{-3}. Given the inherent uncertainty associated with TGA measurements, it is difficult to accurately estimate the number of ester cross-links. However, this ratio (cross-link$_{ester}$/$C_{nanotube}$) might represent a new estimation relating cross-links and mechanical properties.

Figure 5a shows the SEM image of a fractured surface of the condensed-MWCNT films. Films were composed of two-step nanotube layers with many MWCNT ends being observed (Figure 5b). In fact, a fractured surface composed of several-step nanotube layers was observed. It is believed films were composed of several-step nanotube layers resulting from the filtration process of hydrophile-MWCNTs when forming MWCNT films. Hydrophile-MWCNTs gradually aggregated into DMF in the absence of dispersion treatment such as sonication and stirring. As the filtration time passed, the filtration rate of hydrophile-MWCNTs decreased. In this time, nanotubes partially aggregated into DMF and aggregated nanotubes were deposited on the initial MWCNT-deposition film. The tensile stress–strain curve of the condensed-MWCNT and hydrophile-MWCNT films are shown in Figure 6. The tensile stress–strain curve of the condensed-MWCNT films reflects brittle fracture behavior. The tensile measurement of condensed-MWCNT films revealed that the tensile strength to break value was 15 MPa on average, three times stronger than that associated with the hydrophile-MWCNT films (Table 1). On the other hand, the

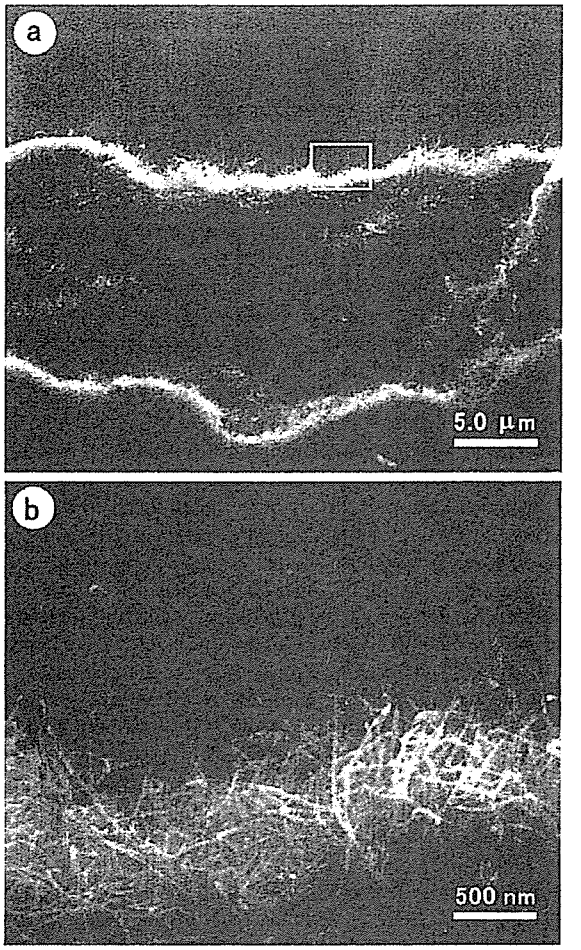

Figure 5. (a) Typical low-magnification SEM image of condensed-MWCNT films. (b) Box in SEM image a shows the border of the SEM image.

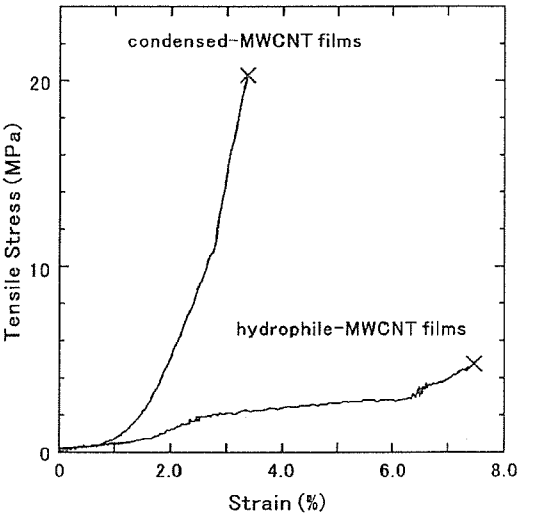

Figure 6. Tensile stress–strain curves of hydrophile-MWCNT and condensed-MWCNT films.

tensile stress–strain curve of the hydrophile-MWCNT films reflects brittle fracture behavior after the tensile stress revealed a constant value in the process of tensile measurement. This type of stress–strain curve was observed in the condensed-MWCNT films with low tensile strength. The tensile strength

TABLE 1: Mechanical Properties of Hydrophile-MWCNT and Condensed-MWCNT Films

	apparent density (g/cm^3)	tensile yield strength (MPa)	elongation to break (%)	Vickers hardness (MPa)	number of cross-links ($bonds/cm^3$)
hydrophile-MWCNT films	0.59	4.8 ± 2.6	6.0 ± 1.5	4.9 ± 0.2	
condensed-MWCNT films	0.59	15 ± 5.2	4.5 ± 1.1	9.2 ± 1.3	1.37×10^{20}

values of condensed-MWCNT films were more scattered than those of the hydrophile-MWCNT films, ranging from 9.7 to 20.2 MPa. This can be attributed to a number of factors including the difficulty in uniformly cross-linking the nanotubes due to the small number of carboxylic acid and hydroxyl groups and the low condensation reaction efficiency. The average elongation to break values, 6.0%, for hydrophile-MWCNT films is 1.3 times in comparison to that for condensed-MWCNT films. This indicates that each nanotube of hydrophile-MWCNT films gives rise to slipping (reflected by the plateau in the stress−strain curve) given the absence of nanotube cross-linking and the load does not transfer all over the films. In the case of condensed-MWCNT films, the improved stress reflects the fact that the stress is transferred to the entire film given the cross-linking of each nanotube. Vickers hardness of samples was estimated by the size of the indentation added by a constant load with a diamond Vickers indenter, where the indentation decreases with increasing hardness. For condensed-MWCNT films, the average Vickers hardness of 9.2 MPa was slightly higher than that of hydrophile-MWCNT films. The hardness can be considered to be the degree of cross-linking between carbon nanotubes. This suggests that the resistance to form indents results from the force dispersion by the presence of cross-linking in the entire condensed-MWCNT films, whereas large indents are simply formed by the concentration of the force at the indenter as hydrophile-MWCNT films represented the only nanotube assembly without cross-linking. Here, an ester cross-linking is formed for 189 carbon atoms of the nanotubes per unit apparent volume of condensed-MWCNT films. If the cross-linking of each nanotube is increased in condensed-MWCNT films, the mechanical properties of the nanotube films would be expected to be even more marked.

Conclusion

In summary, confirmation that MWCNT films cross-linked through ester bonds were prepared by a condensation reaction in the presence of 1,3-dicyclohexylcarbodiimide (DCC) was determined by Fourier transform-infrared spectroscopy. Assuming that the ester bonds are uniformly formed all over the condensed-MWCNT films, the ratio of the number of ester cross-links and carbon atoms of the nanotubes per unit apparent volume (cm^3) of condensed-MWCNT films was 5.27×10^{-3} using TGA. The tensile strength of condensed-MWCNT films achieved an average of 15 MPa, and is 3.1 times in comparison to those of hydrophile-MWCNT films. The mechanical properties of condensed-MWCNT films might be significantly improved through a condensation reaction by making improvements in ester cross-linking such as chemical modifications with a large number of carboxylic acid and hydroxyl groups thereby increasing the amount of condensation through dense contacts between each carbon nanotube.

Acknowledgment. The authors thank Dr M. Ishikuro and Prof. K. Agatsuma for the ICP-OES analysis. This work was supported by a Grant-in-Aid for Basic Research No. (S) 14103016 from the Ministry of Education, Science, Culture and Sport of Japan, Grant No. H18-chemistry-006 from Health and Labor Sciences Research Grants from the Ministry of Health, Labor and Welfare, Tohoku University 21st Century COE Program "International COE of Flow Dynamics", Arai Science and Technology Foundation, and the Collaborative Research from Center for Interdisciplinary Research, Tohoku University.

Supporting Information Available: Purification of multi-walled carbon nanotubes (MWCNTs) sythesized by arc-discharge method. This material is available free of charge via the Internet at http://pubs.acs.org.

References and Notes

(1) Baughman, R. H.; Cui, C.; Zakhidov, A. A.; Iqbal, Z.; Barisci, J. N.; Spinks, G. M.; Wallace, G. G.; Mazzoldi, A.; De Rossi, D.; Rinzler, A. G.; Jaschinski, O.; Roth, S.; Kertesz, M. *Science* **1999**, *284*, 1340.
(2) Kong, J.; Chapline, M. G.; Dai, H. *Adv. Mater.* **2001**, *13*, 1384.
(3) Sreekumar, T. V.; Liu, T.; Kumar, S. *Chem. Mater.* **2003**, *15*, 175.
(4) Zhang, X.; Sreekumar, T. V.; Liu, T.; Kumar, S. *J. Phys. Chem. B* **2004**, *108*, 16435.
(5) Du, C.; Yeh, J.; Pan, N. *J. Mater. Chem.* **2005**, *15*, 548.
(6) Sano, M.; Kamino, A.; Okamura, J.; Shinkai, S. *Science* **2001**, *293*, 1299.
(7) Li, X.; Zhang, J.; Li, Q.; Li, H.; Liu, Z. *Carbon* **2003**, *41*, 598.
(8) Hamon, M. A.; Chen, J.; Hu, H.; Chen, Y.; Itkis, M. E.; Rao, A. M.; Eklund, P. C.; Haddon, R. C. *Adv. Mater.* **1999**, *11*, 834.
(9) Li, Y. H.; Xu, C.; Wei, B.; Zhang, X.; Zheng, M.; Wu. D.; Ajayan. P. M. *Chem. Mater.* **2002**, *14*, 483.
(10) Ishikuro, M.; Sato, Y.; Tohji, K.; Wagatsuma, K. *Bunseki Kagaku* **2006**, *55*, 117.
(11) Prest, W. M.; Mosher, R. A. *Colloids and Surfaces in Reprographic Technology*; Hair, M., Croucher, M.; American Chemical Society: Washington, D. C., 1982; p 255.
(12) Kastner, J.; Winter, J.; Kuzmany, H. *Mater. Sci. Forum* **1995**, *191*, 161.
(13) Shaffer, M. S. P.; Fan, X.; Windle, A. H. *Carbon* **1998**, *36*, 1603.
(14) Sato, Y.; Ogawa, T.; Motomiya, K.; Shinoda, K.; Jeyadevan, B.; Tohji, K.; Kasuya, A.; Nishina, Y. *J. Phys. Chem. B* **2001**, *105*, 3387.
(15) Ros, T. G.; van Dillen, A. J.; Geus, J. W.; Koningsberger, D. C. *Chem. Eur. J.* **2002**, *8*, 1151.
(16) Silverstein, R. M.; Webster, F. X. *Spectrometric Identification of Organic Compounds*, 6th ed.; John Wiley & Sons: New York, 1998.
(17) Otake, Y.; Jenkins, R. B. *Carbon* **1993**, *31*, 109.
(18) Rodriguez, N. M. *J. Mater. Res.* **1993**, *8*, 3233.

Synthesis of Fe-Co Alloy Particles by Modified Polyol Process

D. Kodama[1], K. Shinoda[2], K. Sato[3], Y. Sato[1], B. Jeyadevan[1], and K. Tohji[1]

[1]Graduate School of Environmental Studies, Tohoku University, 6-6-20, Sendai 980-8579, Japan
[2]Institute of Multidisciplinary Research for Advanced Materials, Tohoku University, Sendai 980-8577, Japan
[3]Dowa Mining Company, Tokyo 101-0021, Japan

The successful synthesis of Fe-Co nanoparticles by using a modified polyol process is reported. The formation of the alloy nanoparticles was confirmed by X-ray diffraction and X-ray extended absorption fine structure analyses. The concentration of iron in these particles could be varied between 40% and 90% by controlling the reaction conditions such as initial Fe/Co ratio, reaction temperature and hydroxyl ion concentration. The shape of the particles changed from spherical to cubic when the concentration of Fe was increased from 40 to above 60 at. %. The highest magnetization of 225 emu/g was recorded for $Fe_{70}Co_{30}$ nanoparticles. The magnetization of these particles decreased by about 20% when exposed to severe oxidizing atmosphere for seven days.

Index Terms—**Chemical synthesis, Fe-Co nanoparticles, polyol process, soft magnetic materials.**

I. Introduction

COBALT when alloyed with iron causes an increase in Curie temperature and saturation magnetization. In addition, the alloy possesses low coercivity, low anisotropy and high permeability and is considered for ac and dc devices. Though the synthesis of Fe-Co nanoparticles by thermal decomposition has been reported recently [1], [2], the technique has been very tedious, time consuming, not environment friendly and expensive. On the other hand, Su *et al.* made an attempt to synthesize Fe-Co nanoparticles by reducing the metal ions by hydrazine hydrate and sodium hydroxide in alcohol at room temperature [3]. In 1996, Viau *et al.* [4] made an attempt to synthesize Fe-Co bimetallic particles by polyol process. However, the alloy composition could not be freely manipulated and the maximum concentration of Fe in Fe-Co particles was about 20%. The successful synthesis of Fe-Co nanoparticles can only be realized if the reduction conditions of both Fe and Co are established. The synthesis of Fe particles was considered difficult. On the other hand, the reduction of Co ion in polyol is considered comparatively easy in the presence of hydroxyl ions [5]. Recently, Justin *et al.* reported the reproducible synthesis of Fe by polyol process [6]. In this report, we present the successful synthesis of Fe-Co alloy particles with varying composition by using a modified polyol process. And also we report the magnetic and structural properties of Fe-Co alloy particles.

II. Experiment

A. Synthesis Procedure

Fe-Co alloy particle with varying chemical composition was prepared by using $FeCl_2 \cdot 4H_2O$, $Co(Ac)_2 \cdot 4H_2O$ and NaOH in ethylene glycol (EG). The EG-metal salts-NaOH solution was heated up to the boiling point of EG, refluxed at this temperature for 2 hours and cooled to room temperature. The black precipitate obtained was recovered from polyol and washed and stored in ethanol. The total concentration of metal salts was fixed at 0.01 mol/l, while the Fe:Co molar ratio was varied depending on the target alloy composition. Experimental parameters such as metal ion concentration, hydroxyl ion concentration and reaction temperature were varied to control the size and shape of the particles.

B. Characterization

The morphology of the particles was analyzed by using scanning electron microscope (SEM) and transmission electron microscope (TEM). The composition of the particles was analyzed using X-ray fluorescence and TEM-EDX. The crystal phase and local atomic structures of the magnetic powders were determined by using the X-ray diffractometer (XRD) and extended X-ray absorption fine structure (EXAFS) respectively. The magnetic properties of the particles were measured using a vibrating sample magnetometer (VSM). The stability of the magnetic particles was determined by exposing the powder samples to a highly oxidizing atmosphere and measuring the magnetization at regular time intervals.

III. Results and Discussion

To synthesize pure Fe-Co alloy nanoparticles, the synthesis conditions for co-reduction of Fe and Co metals should be considered. It may be noted that the synthesis of Co particles can be established even at temperatures below the boiling point of polyol. However, the synthesis of the same at temperatures as low as 393 K was not realized. In contrast to this, iron particles with reasonable yield are formed at temperatures as low as 393 K. And also, in the case of Fe-based alloys, a control on the concentration of hydroxyl ion could reduce the gap in the reduction temperature between iron and other metals. If these cannot be tuned well, depending on the reaction temperature, the alloy composition becomes rich in either metal. The synthesis of Fe-Co particles by controlling the hydroxyl ion concentration and reaction temperature to facilitate the co-reduction of Fe

Digital Object Identifier 10.1109/TMAG.2006.880072

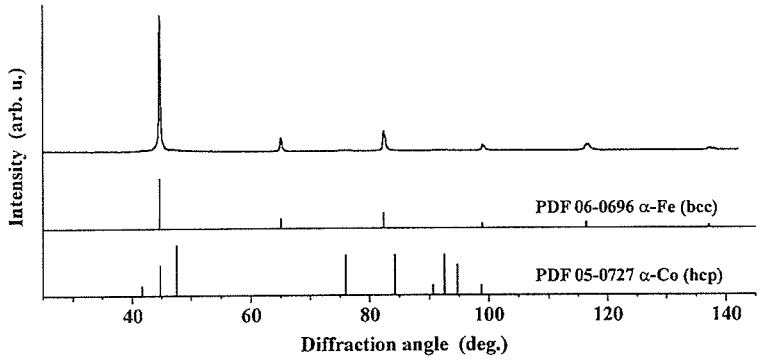

Fig. 1. XRD pattern of the Fe-Co particles synthesized by modified polyol process.

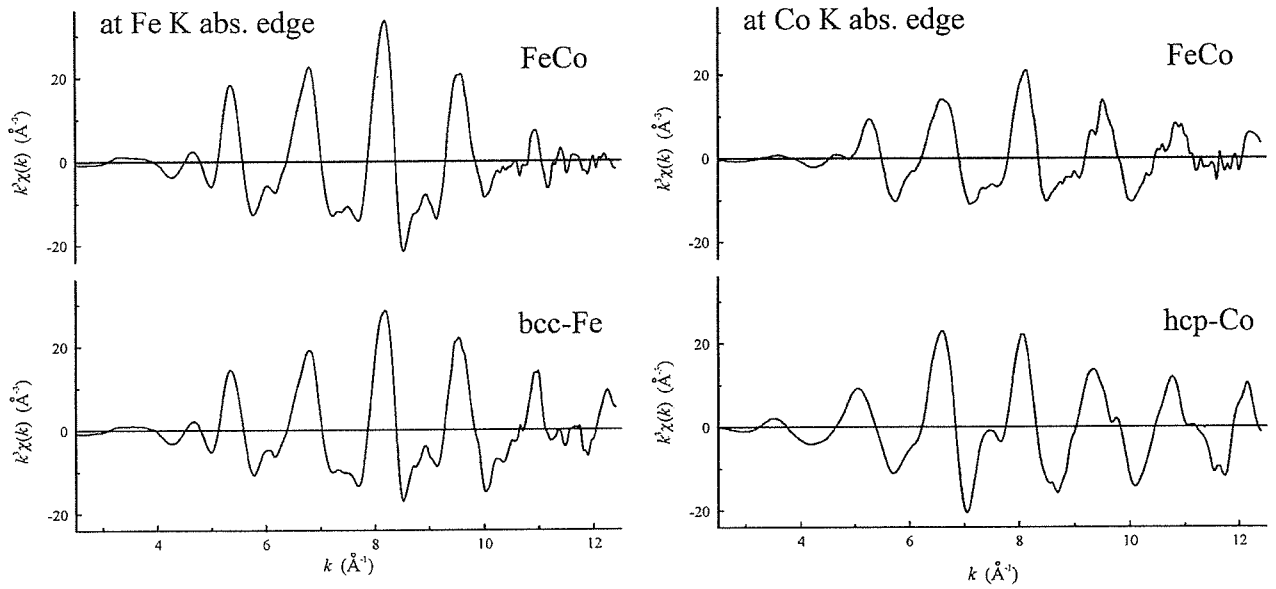

Fig. 2. The k^3 weighted EXAFS spectra at Fe-K and Co-K edges of Fe-Co particles.

and Co was attempted. Though the synthesis of Fe-Co in polyol has been reported in the past using a similar procedure, the results were not convincing enough to confirm the formation of the alloy. Furthermore, even in our study, unfavorable synthesis conditions led to the formation of additional phases such as α-Co and ferrite. To avoid the formation of multiple phases, precautionary measures such as purging the system with nitrogen, controlling the heating rate (to avoid the system remaining at any fixed temperature for an extended period of time), reaction temperature, etc were taken.

The XRD pattern of the particles synthesized under favorable condition by reacting the precursors at the boiling point of polyol is very similar to that of either Fe or Fe-Co [Fig. 1]. On the other hand, the presence of either α-Co or oxide phases was not observed. From the stability of the particles in the atmospheric conditions, the formation of pure Fe was ruled out. However, the samples were analyzed using the EXAFS to understand the structural details.

The EXAFS spectra of the Fe-Co particles at the Fe K (7111 eV) and Co K (7709 eV) absorption edges confirmed the presence of both metals and resembled very much with each other. The plot of $k^3c(k)$ against wave number k of the k^3 weighted fine structure extracted from the absorption spectra of Fe-Co at Fe K edge is very similar to that of the Fe foil and suggests that particles possess the bcc structure as in the case of α-Fe as shown in Fig. 2. On the other hand, the fine structure around Co is obviously different from that of α-Co. Furthermore, similar observations were made from the Fourier transformed profiles, too. In summary, the Fe-Co particles consist of bcc-Fe lattice where part of the Fe atoms is replaced with Co.

The shape, composition and size of Fe-Co nanoparticles are tuned by varying the synthesis conditions such as metal ion concentration, reaction temperature and hydroxyl ion concentration. In other words, the above parameters influence the reaction rate and lead to the variation in shape, which was found to be a function of the concentration of Fe in the particle. The X-ray fluorescence analysis of the particles was carried out to determine the overall composition of the powder. The shape of Fe-Co particles became cubic when they were rich in iron. On the other hand, the shape became spherical in the case of cobalt rich particles. The Fe-Co particles with varying iron concentrations are shown in Fig. 3. The control over the composition of the Fe-Co particles is achieved by controlling the reaction temperature. The reduction of iron and cobalt ions occurs at dif-

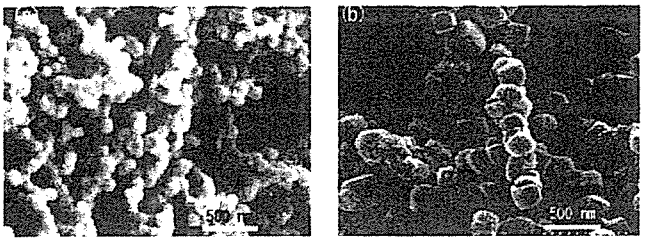

Fig. 3. SEM micrographs of Fe-Co particles synthesized by modified polyol process (a) $Fe_{40}Co_{60}$ and (b) $Fe_{70}Co_{30}$.

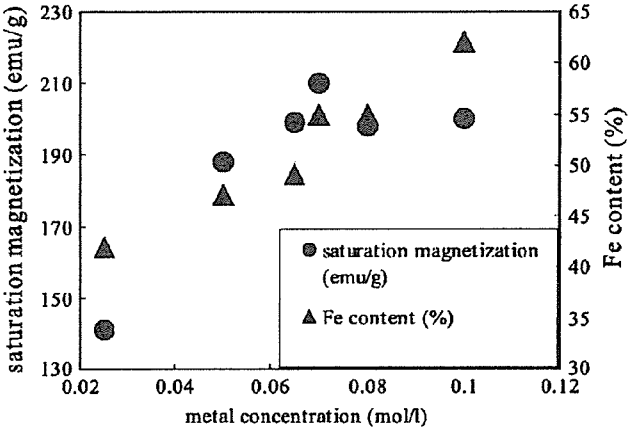

Fig. 4. Relation between Fe content and saturation magnetization.

ferent temperatures. The concentration of iron is high in the particles synthesized at lower reaction temperature and their shape become cubic. The final composition of the Fe-Co particles was easily controlled by varying the initial mole ratio, for particles with Fe concentration ranging between 50 and 90 at.%. Furthermore, above powders have the bcc-iron structures. However, it should be noted that the final concentration of Fe in Fe-Co particles synthesized at higher reaction temperature is always lower irrespective of initial concentration and their shape is nearly

On the other hand, the size of the particles was tuned by controlling the metal ion concentration while maintaining the hydroxyl ion and Fe/Co metal ratio constant. It is believed that the number of nuclei formed is determined very much by the concentration of the hydroxyl ions and the excess metal ions present in the solution are utilized for the growth of these nuclei. Thus, the particle size increases with the increase in metal ion concentration. Though the particle size could be varied between 300 and 50 nm, a detailed investigation is in progress to fully understand the mechanism.

The saturation magnetization of Fe-Co alloy is known to vary depending on the concentration of Fe in the particles showing a maximum close to the Fe:Co ratio of 2:1. The maximum for the bulk Fe_{66} Co_{34} is reported to be 240 emu/g. The saturation magnetization of the Fe-Co particles measured using the VSM under a maximum applied field of 15 kOe is shown in Fig. 4. An anticipated rise in magnetization for particles with higher Fe concentration was recorded and the maximum value obtained for a Fe concentration of 70 at.% was 225 emu/g. Though the

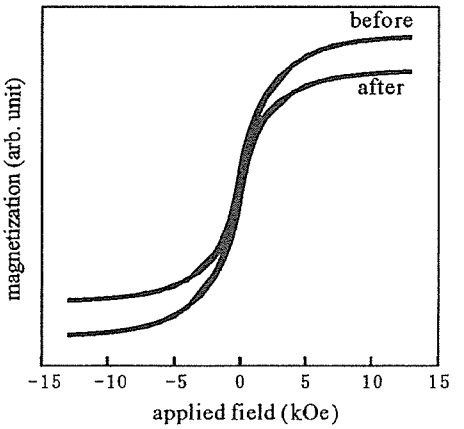

Fig. 5. The magnetic hysteresis loops of FeCo particles before and after subjected to 333 K and 90% humidity for 7 days.

magnetization was lower than that of bulk Fe-Co, it was higher than the value of bulk Fe and also it was very stable compared to iron particles, which get oxidized almost instantaneously.

Though the particles remained fairly stable in ethanol, the long-term stability of the particles is desired from the application point of view. Thus, attempts were made to pacify the surface of the particles by forming a thin oxide layer through controlled oxidation by treating the sample in toluene at specific temperature with a coupling agent. The magnetic hysteresis loops of the sample before and after subjected to 333 K and 90% humidity for seven days is shown in Fig. 5. It could be seen that the drop in saturation magnetization was only 20%. The above result is comparable to the particles considered for any practical application.

ACKNOWLEDGMENT

This work was supported in part by the Ministry of Education, Science, Culture and Sport of Japan and Iketani Science and Technology Foundation #0171078-A under Grant-in-Aid for Basic Research (A) 17201021 and Grant-in-Aid for Basic Research (S) 13852016.

REFERENCES

[1] H. Bönnemann, R. A. Brand, W. Brijoux, H.-W. Hofstadt, M. Frerichs, V. Kempter, W. Maus-Freidrichs, N. Matoussevitch, K. S. Nagabhushana, V. Voights, and V. Caps, *Appl. Organometallic Chem.*, vol. 19, pp. 790–796, Jun. 2005.

[2] C. Desvaux, C. Amiens, P. Fejes, P. Renaud, M. Respaud, P. Lecante, E. Snoeck, and B. Chaudret, *Nature Mater.*, vol. 4, pp. 750–753, Oct. 2005.

[3] X. Su, H. Zheng, Z. Yang, Y. Zhu, and A. Pan, *J. Mater. Sci.*, vol. 38, pp. 4581–4585, Nov. 2003.

[4] G. Viau, F. Fievet-Vincent, and F. Fievet, *J. Mater. Chem.*, vol. 6, no. 6, pp. 1047–1053, Jun. 1996.

[5] F. Fievet, J. P. Lagier, B. Blin, B. beaudoin, and M. Figlarz, *Solid-State Ionics*, vol. 32/33, pp. 198–205, Feb./Mar. 1989.

[6] R. Justin, J. B. Jeyadevan, Y. Sato, K. Tohji, K. Sato, and S. Hisano, "Synthesis of Fe nanoparticles through polyol process," in *Proc. 28th Annu. Conf. Magnetics in Japan*, Okinawa, Japan, Sep. 2004, p. 38.

Manuscript received March 12, 2006; revised June 20, 2006 (e-mail: jeya@mail.kankyo.Tohoku.ac.jp).

Polyol Process for Fe-Based Hard(fct-FePt) and Soft(FeCo) Magnetic Nanoparticles

B. Jeyadevan[1], K. Shinoda[2], R. J. Justin[1], T. Matsumoto[2], K. Sato[3], H. Takahashi[1], Y. Sato[1], and K. Tohji[1]

[1]Graduate School of Environmental Studies, Tohoku University, Sendai 980-8579, Japan
[2]Institute of Multidisciplinary Research for Advanced Materials, Tohoku University, Sendai 980-8577, Japan
[3]Dowa Mining Company, Chiyoda-ku, Tokyo 101-0021, Japan

The polyol process and the parameters influencing the synthesis of metal and alloy nanoparticle are discussed. Then, the synthesis strategies to obtain hard (Fe–Pt) and soft (Fe–Co) nanoparticles by using polyol process is presented. Under optimum synthesis conditions, partially ordered Fe–Pt nanoparticles with an average grain diameter of 8 nm exhibited a coercivity of 460 kA/m in the as-synthesized state. In the case of Fe–Co alloy particles, synthesis technique to prepare particles with varying Fe concentration in the size ranging between 300 and 50 nm is reported.

Index Terms—**Co alloys, FeCo, FePt, polyol process, soft magnetic materials.**

I. Introduction

THE synthesis of monodispersed metal and alloy nanoparticles is of fundamental importance for the development of novel technologies based on the properties of the particles themselves as well as nanostructure derivatives fabricated using the same. This holds true for nonmagnetic particles such as gold, silver, and copper and also for ferromagnetic metals and alloys. Though the synthesis of nanoparticles as well as nanostructures using the dry process dominated for the last ten to 15 years that led to considerable development in science and technology, the use of solution techniques have made a comeback and has demonstrated its potential in the synthesis of monodispersed oxides, metal and alloy nanoparticles, and their assemblies [1]–[3]. Particularly, considerable progress has been made in the synthesis of hard and soft magnetic nanoparticles using solution techniques [4], [5]. As most of the novel applications demand the use of either metal or alloy nanoparticles, synthesis of the same by using nonaqueous process is preferred over the aqueous counter part. Although thermal decomposition process is very often used for the synthesis of metal and alloy nanoparticles, the coproduction of highly toxic carbon monoxide on one hand and the difference between decomposition temperatures of metallic compounds in the cases of alloy particles synthesis on the other, make this process environmentally very unfriendly and complicated. In some cases, the process extends over a period of three to four days to synthesize alloy nanoparticles [6]. On the contrary, the reduction of metal salts using polyol, which acts as a solvent and reducing and oxidation protecting agents in the case of metal and alloy particle synthesis has been demonstrated to be comparatively environmentally friendly and simple [7]. The authors have succeeded in the synthesis of ferromagnetic metal and alloy nanoparticles by using the polyol process and demonstrated the potential of this process in obtaining nonmagnetic as well as magnetic nanoparticles with outstanding properties [8]–[10]. In this paper, we discuss the polyol process and report the synthesis strategies and properties of Fe–Pt and Fe–Co nanoparticles using the aforementioned process.

II. Polyol Process

A. Reaction Process in Polyols

In polyol process, metal species are chemically reduced in liquid polyol. In this process, the metal salts are dissolved in liquid polyol in an inert atmosphere and heated to elevated temperatures to obtain fine metal or alloy nanoparticles [11]–[13]. The reduction of metal hydroxides to metals takes place through dehydration and oxidation reactions as given in (1) and (2) in ethylene glycol (EG) [14]

$$2CH_2OH{-}CH_2OH \rightarrow 2CH_3CHO + 2H_2O \quad (1)$$

$$2CH_3CHO + M(OH)_2 \rightarrow CH_3COCOCH_3 + 2H_2O + M^{\circ}. \quad (2)$$

In the case of reduction of metal oxides in boiling EG, the reduction reaction proceeds as

$$C_2H_6O_{2(l)} + 5/xMO_{x(s)} \rightarrow 5/xM^{\circ}_{(s)} + 2CO_{2(g)} + 3H_2O_{(g)}. \quad (3)$$

However, in the case of reduction from other metal complexes or compounds, the process may follow a different path depending on the type of precursors and polyols. The reaction rate (r) of the polyol process determines the properties of nanoparticles such as size and its distribution, crystal structure, etc. and is a function of various experimental parameters described by the equation given as follows

$$r = f(P_{\mathrm{redox}}, M_{\mathrm{conc.}}, H_{\mathrm{conc.}}, T_{\mathrm{reac.}}) \quad (4)$$

where, P_{redox}; the reduction potential of polyol, $M_{\mathrm{conc.}}$; the metal ion concentration, $H_{\mathrm{conc.}}$; the concentration of hydroxyl ions, $T_{\mathrm{reac.}}$; the reaction temperature.

When the P_{redox} of the polyol is high, the size of the particles becomes smaller, provided that the rest of the conditions remain constant. Here, the metal ions are reduced rapidly forming an avalanche of nuclei consuming a large portion of the metal

Digital Object Identifier 10.1109/TMAG.2006.880149

species and the particle diameter is consequently small due to the limited supply of metal ions for growth. The authors made an attempt to evaluate the reduction potentials of polyols by measuring the natural potential using silver as reference electrode. However, the presence of impurities swayed the results of similar polyols produced by different manufacturers. The main reason for this was the inability to measure the potential difference between salt bridge and polyol [15]. Furthermore, the reduction potential of the polyol increases with temperature and reaches its maximum at the boiling point. However, this increment with temperature varied between polyols and made the prediction of the reduction potential of polyols at boiling point difficult. On the other hand, an attempt was made to evaluate the reduction potential of polyol by using the molecular orbital theory [16]. The reduction of metal ion is realized in polyol through the electron transfer between metal and polyol. The decisive factor during this reaction is the orbital energy levels possessed by the metal ions and polyol. Here, the orbit and orbital energy were calculated by using quantum chemistry and the reduction reaction is believed to progress through HOMO and LUMO orbits possessed by polyol and the metal, respectively. At the same time, it is important to select the appropriate orbital levels for the reduction of metal ions. To determine the orbital levels, we have calculated different types of polyol fixing the metal ion and succeeded in determining the reducibility of polyols. The reducing potentials in the increasing order for some of the promising polyols used in nanoparticles synthesis are tetraethylene glycol (TEG), ethylene glycol (EG) and trimethylene glycol (TMEG). The results were in agreement with the experimental observations in the synthesis of nonmagnetic as well as magnetic particles.

The reaction rate (r) could also be enhanced by either increasing the metal ion concentration (M_{conc}) or raising the temperature (T_{reac}). However, the properties of the product such as particle size cannot be predicted easily as other factors such as H_{conc} and P_{redox} indirectly influence the outcome. Furthermore, the reaction rate is enhanced when the H_{conc} in metal ion—polyol system is increased. The concentration of hydroxyl ions (OH^-) necessary for the reduction of metal ions in polyol is also a function of the type of polyol. Highly reducing polyols need lesser amounts of OH^- to synthesize particles of comparable diameters. The presence of OH^- in the metal ion-polyol system is believed to act as a catalyst in accelerating the formation of precursor complexes. The formation of such complexes is believed to occur at lower temperatures in the presence of OH^-. However, this has not been experimentally verified till now. An attempt was made to verify the same by monitoring the UV-visible spectra of the metal ion—polyol—hydroxyl ion system under various reaction temperatures. The representative results of the aforementioned study are shown in Fig. 1. Here, the reduction of cobalt acetate to form Co in EG goes through an intermediate metal complex formation step at boiling point in the absence of hydroxyl ions, whereas similar complex forms at a lower temperature in the presence of hydroxyl ions as shown by the arrow marks in Fig. 1. The type of polyol and metal salts also influences the conditions at which these intermediates are formed. A detailed study of the reduction process of Co in polyol is in progress.

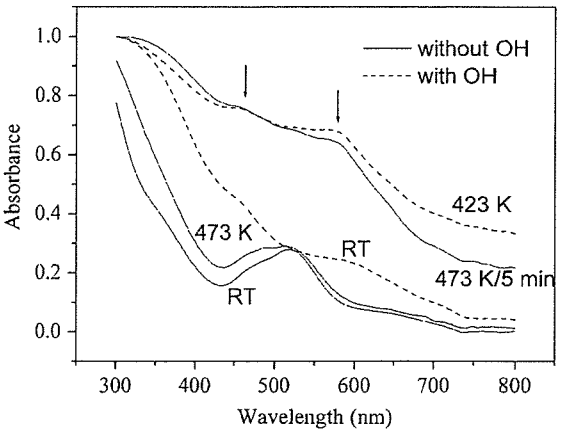

Fig. 1. UV-Visible spectrum showing the effect of OH on the formation of Co-complex with temperature.

B. Formation of Alloys in Polyols

In polyol process, the reduction of noble metals like Ag, Au, and Pt and its alloys and some transition metals such as Co, Ni, and Cu have also been materialized with relative ease. Unlike in the case of pure metals, the formation of binary alloys has to satisfy the basic requirements of coreduction of the metal ions in question. The failure to reduce the metal ions together would result in the formation of separate metal entities or in the reduction of one of the two metals. There are two possible routes through which one could succeed in the synthesis of alloy nanoparticles [14]. In the first case, the alloys are formed when the oxidation reduction potentials of the metals are comparable, for example, Ni and Co. However, it should be noted that this argument is valid only when both the metal ions prevail in the reducible form in solution. For example, the synthesis of Co metal in EG is achieved with the cobalt acetate and not with cobalt chloride under similar experimental conditions. The easiness with which the metal salts form complexes differs and this may influence the formation of alloys. However, marginal differences may lead to the formation of alloys of core-shell structures, where core and the shell can be rich in either metal. In the second case, the alloys are formed when one metal that get reduced easily acts as a catalyst and assists the reduction of the other which is otherwise hard to get reduced. Such a situation prevails in the case of noble metal based alloys such as Fe–Pt, Co–Pt, etc. However, in this case too, the appropriate selection of the metal salts is vital and they should dissociate at specific temperatures where the reduction of both metals is possible. Although, the synthesis of magnetic transition metal particles such as Co and Ni has been comparatively straightforward, the formation of transition alloy such as Fe–Co and Fe–Ni with desired composition using polyol process has been a challenge. However, we have been successful in the synthesis of hard and soft magnetic alloys by using polyol process. The synthesis strategies and properties of Fe–Pt and Fe–Co nanoparticles are described here in after.

III. Synthesis and Properties of Hard (fct-FePt) and Soft (FeCo) Nanoparticles

A. Synthesis of Fe–Pt Nanoparticles

Chemical synthesis of self-assembled, monodispersed, and chemically ordered $L1_0$ FePt and CoPt nanoparticles for ul-

trahigh density magnetic storage [17]–[20] gained momentum soon after the report by Sun *et al.* in the year 2000. The ordered $L1_0$ phase of these systems possesses high magnetocrystalline anisotropy (K_u) and allows the use of thermally stable particles with 4-5 nm in diameter [17] as the basic unit for recording. The particles synthesized using the thermal decomposition technique is reported to be superparamagnetic, chemically disordered, fcc in structure [17], and need to be annealed at 853 K to obtain the $L1_0$ structure. However, the annealing step induces coalescence of nanoparticles and works negatively for achieving high recording density. Therefore, concerted effort was made to lower the transition temperature (T_t) by adding a third element (eg. Cu, Sn, Pb, Sb, Ag, and Bi) that lower the T_t through surface segregation [21], [22]. However, the reduction of T_t was limited to temperatures around 673 K and further reduction remained a challenge. On the other hand, if we consider the crystal structure of Fe–Pt, the ordered fct structure is the stable phase against metastable chemically disordered fcc structure. In nanoparticles, surface energy that constitutes a large part of the total free energy can be a significant factor in structure determination. Furthermore, the activation barriers to phase transformations are relatively low in very small particles [23]. This phenomenon gives rise to complex coupled growth-phase transformation behavior in nanoparticles. For example, the bulk Co is known to have fcc phase at temperatures as high as 694.5 K. Authors in synthesizing Co metal particles using the chemical route, namely modified polyol process [8], obtained the following: the particles chemically synthesized at temperatures as low as 468 K were found to possess fcc structure at micrometer size levels. When the reaction kinetics was enhanced, the particle size was reduced to submicrometer and even to a few tens of nanometers. Along with size reduction, the crystal structure also changed from fcc at micrometer size range, a mixture of fcc and hcp in the submicrometer size range and to epsilon and hcp Co at nanometer size range [24]. The size reduction is a consequence of fast reaction kinetics and so the formation of unstable phases. Hence, during synthesis, the nanoparticles seem to undergo the formation of unstable phases and by controlling the reaction kinetics, different particle sizes and crystal structures can be realized. In other words, the formation of most stable phase could be realized by maintaining low reaction rate or mild reaction conditions.

If we consider the method used for the synthesis of Fe–Pt particles by IBM, the Fe and Pt atoms for the formation of the particles are supplied by thermal decomposition of iron carbonyl and reduction of platinum salts by polyol, respectively. Since the release of iron through thermal decomposition is very rapid, similar rate has to be maintained in supplying platinum also for the formation of Fe–Pt alloy. The high reduction rate of platinum has been achieved through the use of highly reducing solvent such as 1, 2-hexadecanediol. This leads to fast reaction rate and consequently to unstable disordered fcc-FePt. On the contrary, if the synthesis of Fe–Pt using polyol process is attempted, Fe and Pt salts that are reduceable at about the same temperatures should be selected to facilitate coreduction. For example, the use of hexachloroplatinate is not suitable to be used with iron acetyl acetonate. Here, the platinum will be reduced prior to the dissociation of iron and the coreduction will not be realized. Thus, we have to select a platinum salt that dissociates at higher temperature than the iron counterpart to realize the formation of Fe–Pt particles. The synthesis of Fe–Pt particles was carried out using Fe and platinum acetylacetonates as starting materials [25]. Furthermore, the reaction was carried out in tetraethylene glycol, which has low reduction potential compared to EG or TMEG. The slow reaction rate in TEG compared to other polyols resulted in the formation of significantly ordered Fe–Pt nanoparticles above 553 K. The ordering also resulted in high intrinsic coercive field of nearly 2.47 MA/m. The room temperature (RT) and low temperature (5 K) magnetic loops of Fe–Pt particles synthesized at 473 K in TEG are shown in Fig. 2. The particles show a coercivity value of 143 kA/m at 5 K. Since the size of these particles is below the superparamagnetic limit, room-temperature magnetization does not show any coercivity. Furthermore, the particles synthesized in TEG form a petal-like structure, which is not observed in the case of other polyols, facilitates the sintering and subsequent growth, and finally ferromagnetic features at 563 K. It is believed that the mild reaction conditions and also the sintering of the particles are the main causes for the partial ordering in the Fe–Pt samples synthesized in TEG.

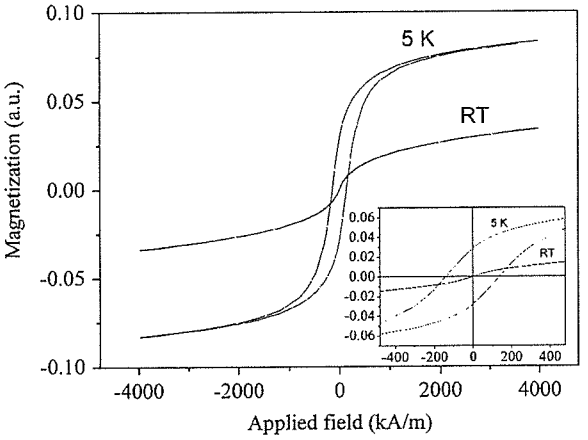

Fig. 2. RT and 5 K hysteresis loop of FePt nanoparticles synthesized in TEG at 473 K. Inset shows the magnified portion of the loops.

When the Ni nanoparticles were synthesized in TEG, the particles formed initially were fcc in structure; however, they were converted to hcp at higher temperatures and remained stable even at the boiling point of TEG. It was observed that the crystal structure change has been associated with sintering. The degree of transformation depended on the size of the initial fcc Ni particles and a complete transformation was achieved at lower temperature when the initial particle size was smaller. It should also be noted that though the ordering of the Fe–Pt was associated with sintering, the degree of ordering depended on the ordered state of the primary Fe–Pt particles. It is believed that the sintering will result in polycrystalline particles, which are not suitable for recording purposes, and the synthesis process was modified by introducing few percentage of hexachloroplatinate and carboxylic acid as nucleating and complex agents [26]. This was expected to inhibit the formation of petal-like structure and facilitate growth. The fluctuation in the physical properties of the particles was subdued and the average grain size of the

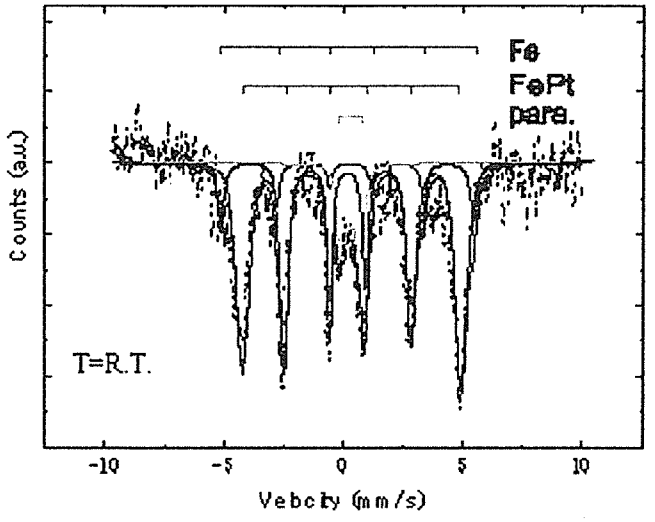

Fig. 3. Mössbauer spectrum at RT for the as-prepared FePt.

particles at 473 K was only 3.4 nm and agreed well with the transmission electron microscopy (TEM) observation. Though the particles synthesized at 573 K were difficult to be dispersed and observed in TEM, the grain size estimated from X-ray was 8 nm and suggested growth through sintering. As it was difficult to disperse these particles in organic solvent, the observation in TEM or estimation of the size distribution was not possible. The crystal structures of flower petal-like structured Fe–Pt particles synthesized in TEG at 473 K and Fe–Pt particles synthesized using 1% H_2PtCl_6 and five equivalent weight of iron of carboxylic acid to facilitate growth and prevention of petal-like structure were analyzed using X-ray diffraction (XRD), extended X-ray absorption fine structure (EXAFS), and anomalous small-angle X-ray scattering (ASAXS). to understand the macro— and micro-structure of Fe–Pt particles. The results suggest that the particles synthesized at 473 K consisted of Pt rich Fe–Pt core and amorphous shell rich in Fe. However, when these particles are annealed in TEG at 573 K, sintering of these particles occur at the amorphous interface and crystallization progresses along with ordering resulting in the formation of partially ordered ferromagnetic Fe–Pt. The details are reported in [27]. The particles synthesized under optimum condition exhibited a coercivity of 460 kA/m and anisotropy field of over 3.18 MA/m. The superlattice reflection lines of (001) and (110) from the XRD confirmed the presence of fct-FePt. The room-temperature Mössbauer spectrum of particles with Fe:Pt ratio of 52.5:47.5 is shown in Fig. 3. From these results, the ordered fraction in the sample was estimated to be more than 50%. The spectrum was fitted with two sextets and a superparamagnetic doublet. The sextet with low hyperfine field value of 28.55 (±0.30) T represents fct-FePt, whereas the second sextet with the hyperfine field (33.05 T) close to that of Fe suggests the presence of Fe rich environment in FePt.

Though the magnetic properties of the particles synthesized using the above process exhibited properties superior to the ones synthesized using the IBM method, these particles could not be dispersed into suspension to analyze their morphology in detail to better understand the ordering process. The major obstacle is thought to be the stained surface of Fe–Pt with polymerized TEG. Therefore, it is necessary to develop a method modifying the polyol process that enables the synthesis of particles larger than the superparamagnetic diameter at lower temperature.

As discussed earlier, the present method is devised on the presumption that it is difficult to reduce iron at lower temperatures in polyol. Since we have developed the technology to reduce iron at temperatures as low as 393 K, the coreduction of iron and platinum using iron chloride and hexachloroplatinate has become feasible [28]. Currently, efforts are made to synthesize Fe–Pt particles with diameter larger than the superparamagnetic limit, which would facilitate highly ordered Fe–Pt particles.

B. Synthesis of Fe–Co Nanoparticles

Viau *et al.* attempted the synthesis of Fe–Co alloy particles in polyol in 1996 [10]. In their paper, it is reported that the formation of iron-based polymetallic particles was based on the preposition that the metallic iron powders is synthesized by disproportionation of iron hydroxide in organic media with the concomitant reduction of other metal hydroxides such as Co and Ni in the original process. It is also claimed that the polyol process does not apply to iron as it is more electropositive than Ni or Co and polyols are too weak to reduce ferrous ions. If iron is synthesized through disproportionation, we should obtain equal quantities of metallic iron and magnetite. However, it is claimed that the crystallization of magnetite could be prevented by: 1) limiting the initial concentration of ferric ions to 0.2 mol.dm^{-3}; 2) adding excess amount of hydroxyl ions; and 3) the system should be free from water. However, authors are of the opinion that the polyol do have the potential to reduce iron and the synthesis of iron metal as well as low-temperature synthesis of Fe-based noble and transition metal alloys in polyol is feasible.

Though the synthesis of micrometer-sized metal iron in polyol was reported in 1996, no one has either confirmed or reproduced their findings. Recently, we attempted the synthesis of iron nanoparticles in polyols and succeeded in obtaining the particles only when iron chloride was used as starting material as claimed by Viau *et al.* However, the yield of metal iron and oxide fraction varied depending on the reducing potential of the polyols. Furthermore, the grain size of the iron nanoparticles synthesized using highly reducing polyol such as TMEG was small compared to the ones prepared using EG. In addition, the X-ray diffraction lines of magnetite were less intense in the product containing large size grains suggesting that the magnetite is formed through the oxidation of iron and not as a product of the disproportionation reaction. A detailed report on the synthesis of iron nanoparticles and the low-temperature synthesis of Fe-based alloy nanoparticles are presented in [28] and [29].

Our successful attempt to synthesize iron in polyol and the proposition that the polyol has the necessary potential to reduce iron salts motivated us to make a fresh attempt on the synthesis of Fe-based transition metal alloys such as Fe–Co and Fe–Ni. Here, we discuss some of our results on the synthesis of Fe–Co nanoparticles using polyol process.

As stated earlier, though the synthesis of Fe–Co in polyol was claimed nearly a decade ago, the powders were polyphasic and also made up of polydispersed agglomerates of Fe and Co particles. Also, the composition could not be freely manipulated and the concentration of iron in the powder was a maximum of about

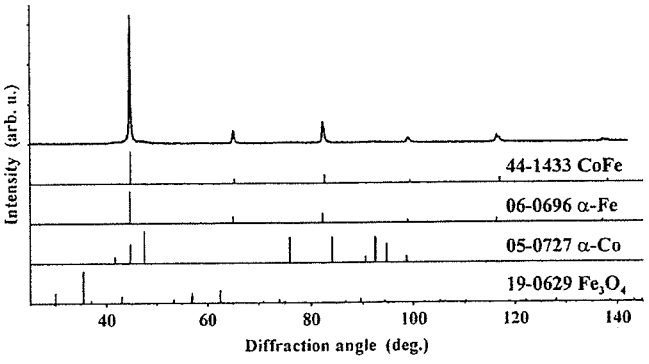

Fig. 4. XRD profile of $Fe_{40}Co_{60}$ particle using Cu-K_α.

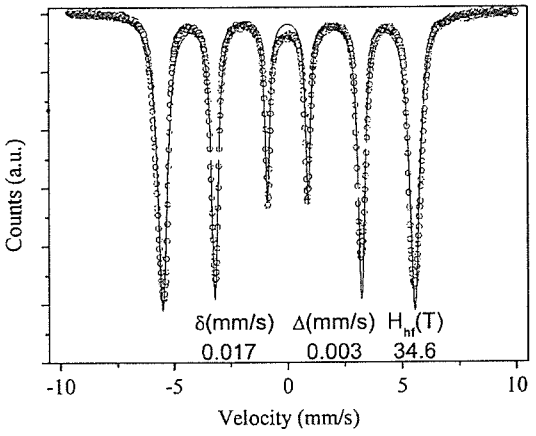

Fig. 5. Room-temperature Mössbauer spectrum of $Fe_{85}Co_{15}$ alloy synthesized in EG.

Fig. 6. SEM micrographs of the FeCo alloy nanoparticles (a) $Fe_{73}Co_{23}$, (b) $Fe_{74}Co_{26}$, and (c) $Fe_{57}Co_{43}$ synthesized in EG.

20%. Taking into account of the fact that the polyol has the potential to reduce iron, especially at temperatures well below the boiling point of the solvent, a fresh attempt was made to synthesize Fe–Co nanoparticles with varying sizes and composition.

The Fe–Co alloy powder samples were synthesized using $FeCl_2{\cdot}4H_2O$, $Co(Ac)_2{\cdot}4H_2O$ (Ac=acetate) salts and NaOH in ethylene glycol (EG), which acts as a solvent and reducing agent and reacting them at different temperatures to arrive at the required Fe/Co ratio. The formation of multiple phases such as metals, alloys and oxides are observed in the powders synthesized under the normal preparative conditions. However, in the modified process the particles consist of only Fe–Co alloy phase as shown in Fig. 4. The potential of this method could be appreciated only if the control over the composition, size, size distribution and shape of the alloy is accomplished. The authors have already reported the synthesis of Co metal particles with different sizes and crystal structures using polyol process in 2004 [24]. Here, it may be noted that the synthesis of Co particles can be established even at temperatures below the boiling point of polyol. However, the synthesis of the same at temperatures as low as 393 K was not realized. In contrast to this, the iron particles with reasonable yield are formed at temperatures as low as 393 K. And also, in the case of Fe-based alloys, a control on the concentration of hydroxyl ion could reduce the gap in the reduction temperature between iron and other metals [28]. If these cannot be tuned well, depending on the reduction temperature at which we operate, the alloy composition becomes rich in either metal. This was clearly observed in the case of Fe–Co synthesis and the particles became rich in iron at lower reduction temperature, whereas it was rich in Co at higher reduction temperature. The reason for this is believed to be due to the intermediate compounds formed by Fe and Co as well as their stabilities against temperature. The authors are of the opinion that the iron compound or complex formed at lower temperatures requires less potential than that of Co. Thus, iron is reduced at lower temperatures at which the polyol does not have the necessary potential to reduce Co. However, at elevated temperatures, the reduction of Co is enhanced very much compared to Fe, leading to Co rich Fe–Co alloy. Thus, the Fe-rich and Co-rich alloys could be achieved through the control of the reduction temperature. Fig. 5 shows the Mössbauer spectrum of the $Fe_{85}Co_{15}$ alloy (composition from X-ray fluorescence) synthesized at 403 K. The large hyperfine field of 34.6 T compared to 33.0 T for Fe suggests the formation of Fe–Co alloy particles. The size distribution of these particles has been comparatively narrow. The morphology of the particles is cubic as seen in Fig. 6 which is influenced by the concentration of Fe in the particles. Additional details on the synthesis and identification of Fe–Co phase using XRD and EXAFS are available in the paper reported by Kodama *et al.* [30].

Another area where we need control to acclaim the potential of this process is the control over particle size. If we recall the classical paper by LaMer [31], the only way to have control over the particle size as well as distribution is to separate out the nucleation and growth steps during the synthesis. In simple terms, the particle size can be tuned by varying the metal ion concentration. However, the rise in metal ion concentration should not prolong over the period of nucleation, which will consequently influence the distribution of the particle size. As discussed in Section II, the hydroxyl ion concentration plays an important role in determining the nucleation rate. Thus manipulating the hydroxyl ion concentration can control the number of nuclei formed in any system. Fig. 6. shows the SEM micrographs of iron-rich Fe–Co particles with various sizes ranging between 300 and 50 nm. The authors believe that further reduction in size is possible through a finer control over the experimental conditions and work is in progress in similar direction. Also, we are investigating the possibilities of using iron-rich Fe–Co alloy particles for high-frequency application.

ACKNOWLEDGMENT

This work was supported in part by the Ministry of Education, Science, Culture, and Sport of Japan under Grant-in-Aid

for Basic Research (A) 17201021, and (S)13852016. The authors would like to thank Dr. M. Doi for the Mössbauer measurements.

REFERENCES

[1] T. Hyeon, "Chemical synthesis of magnetic nanoparticles," *Chem. Commun.*, pp. 927–934, 2003.

[2] M. A. Willard, L. K. Kurihara, E. E. Carpenter, S. Calvin, and V. G. Harris, "Chemically prepared magnetic nanoparticles," *Int. Mater. Rev.*, vol. 49, pp. 125–170, 2004.

[3] M. Giersig and M. Hilgendorff, "Magnetic nanoparticle superstructures," *Eur. J. Inorg. Chem.*, pp. 3571–3583, 2005.

[4] S. Sun, "Recent advances in chemical synthesis, self-assembly and applications of FePt nanoparticles," *Adv. Mater.*, vol. 18, pp. 393–403, 2006.

[5] C. Desvaux, C. Amiens, P. Fejes, P. Renaud, M. Respaud, P. Lecante, E. Snoeck, and B. Chaudret, "Multimillimetre-large superlattices of air-stable iron–cobalt nanoparticles," *Nature Mat.*, vol. 4, pp. 750–753, 2005.

[6] H. Bonnemann, R. A. Brand, W. Brijoux, H.-W. Hofstadt, M. Frerichs, V. Kempter, W. Maus-Friedrichs, N. Matoussevitch, K. S. Nagabhushana, F. Voigts, and V. Caps, "Air stable Fe and Fe–Co magnetic fluids-synthesis and characterization," *App. Organometallic Chem.*, vol. 19, pp. 790–796, 2005.

[7] F. Fievet, J. P. Lagier, B. Blin, B. Beaudoin, and M. Figlarz, "Homogeneous and heterogeneous nucleations in the polyol process for the preparation of sub-micron size metal particles," *Sol. State Ionics*, vol. 32, pp. 198–205, 1989.

[8] T. Hinotsu, B. Jeyadevan, C. N. Chinnasamy, K. Shinoda, and K. Tohji, "Size and structure control of magnetic nanoparticles by using a modified polyol process," *J. Appl. Phys.*, vol. 95, pp. 7477–7479, 2004.

[9] C. N. Chinnasamy, B. Jeyadevan, K. Shinoda, K. Tohji, A. Narayanasamy, K. Sato, and S. Hisano, "Synthesis and magnetic properties of face-centered-cubic and hexagonal-close-packed Ni nanoparticles through polyol process," *J. Appl. Phys.*, vol. 97, p. 10J309, 2005.

[10] M. Takahashi, T. Ogawa, D. Hasegawa, and B. Jeyadevan, "Direct synthesis of Pt based L1(0) structured nanoparticles," *J. Appl. Phys.*, vol. 97, p. 10J307, 2005.

[11] G. Viau, F. Fieve-Vincent, and F. Fievet, "Monodisperse iron-based particles: Precipitation in liquid polyols," *J. Mater. Chem.*, vol. 6, pp. 1047–1053, 1996.

[12] G. Viau, F. Fievet-Vincent, and F. Fievet, "Nucleation and growth of bimetallic CoNi and FeNi monodisperse particles prepared in polyols," *Solid State Ionics*, vol. 84, pp. 259–270, 1996.

[13] G. Viau, R. Brayner, L. Poul, N. Chakroune, E. Lacaze, F. Fievet-Vincent, and F. Fievet, "Ruthenium nanoparticles: Size, shape, and self-assemblies," *Chem. Mater.*, vol. 15, pp. 486–494, 2003.

[14] D. Larcher and R. Patrice, "Preparation of metallic powders and alloys in polyol media: A thermodynamic approach," *J. Sol. State Chem.*, vol. 154, pp. 405–411, 2000.

[15] K. Urakawa, "Synthesis of FePt nanoparticles suitable for magnetic recording media," M.S. thesis, Tohoku Univ., Sendai, Japan, 2005. (In Japanese).

[16] T. Matsumoto *et al.*, Estimation of the reduction potential of polyol by using molecular orbital theory. unpublished.

[17] S. Sun, C. B. Murray, D. Weller, L. Folks, and A. Moser, "Monodisperse FePt nanoparticles and ferromagnetic FePt nanocrystal superlattices," *Science*, vol. 287, pp. 1989–1992, 2000.

[18] C. N. Chinnasamy, B. Jeyadevan, K. Shinoda, and K. Tohji, "Polyol-process-derived CoPt nanoparticles: Structural and magnetic properties," *J. Appl. Phys.*, vol. 93, pp. 7583–7585, 2003.

[19] C. Liu, X. Wu, T. Klemmer, N. Shukla, X. Yang, D. Weller, A. G. Roy, M. Tanase, and D. Laughlin, "Polyol process synthesis of monodispersed FePt nanoparticles," *J. Phys. Chem. B*, vol. 108, pp. 6121–6123, 2004.

[20] Y. Ding and S. A. Majetich, "Size dependence, nucleation, and phase transformation of FePt nanoparticles," *App. Phys. Lett.*, vol. 87, p. 22508, 2005.

[21] J. W. Harrell, D. E. Nikles, S. S. Kang, X. C. Sun, Z. Jia, S. Shi, J. Lawson, G. B. Thompson, C. Srivastava, and N. V. Seetala, "Effect of metal additives on L1(0) ordering of chemically synthesized FePt nanoparticles," *Scripta Mater.*, vol. 53, pp. 411–416, 2005.

[22] O. Kitakami, Y. Shimada, K. Oikawa, H. Daimon, and K. Fukamichi, "Low-temperature ordering of L1(0)-CoPt thin films promoted by Sn, Pb, Sb, and Bi additives," *Appl. Phys. Lett.*, vol. 78, pp. 1104–1106, 2001.

[23] A. A. Gribb and J. F. Banfield, "Particle size effects on transformation kinetics and phase stability in nanocrystalline TiO_2," *Am. Mine.*, vol. 82, pp. 717–728, 1997.

[24] O. Perales-Perez, B. Jeyadevan, C. N. Chinnasamy, K. Tohji, and A. Kasuya, *Inorganic Materials: Recent Advances*, D. Bahadur, S. Vitta, and O. Prakash, Eds. New Delhi, India: Narosha, 2004, p. 9.

[25] B. Jeyadavan, K. Urakawa, A. Hobo, N. Chinnasamy, K. Shinoda, K. Tohji, D. D. J. Djayaprawira, M. Tsunoda, and M. Takahashi, "Direct synthesis of fct-FePt nanoparticles by chemical route," *Jpn. J. Appl. Phys.*, vol. 42, pp. L350–352, 2003.

[26] S. Hisano, K. Sato, K. Urakawa, B. Jeyadevan, and K. Tohji, "Effect of additives on the direct synthesis of $L1_o$-FePt nanoparticles by polyol process," *J. Magn. Soc. Jpn.*, vol. 29, 2005.

[27] K. Shinoda, K. Sato, J. Balachandran, and K. Tohji, "Local structure of directly synthesized LIo FePt nanoparticles," *Intermag*, 2006.

[28] R. J. Joseyphus, B. Jeyadevan, K. Shinoda, Y. Sato, and K. Tohji, "Low temperature synthesis of Fe and Fe-based alloys," *Proc. ISHR and ICSTR*, Aug. 5–9, 2006.

[29] R. Justin Joseyphus *et al.*, "Role of polyol in the synthesis of Fe particles," in *Proc. ICM*, Kyoto, Japan, Aug. 20–25, 2006.

[30] J. Balachandran, D. Kodama, K. Shinoda, K. Sato, Y. Sato, and K. Tohji, "Synthesis of FeCo alloy particles by modified polyol process and their structural and magnetic properties," *Intermag*, 2006.

[31] V. K. LaMer and R. H. Dinegar, "Theory, production and mechanism of formation of monodispersed hydrosols," *J. Am. Chem. Soc.*, vol. 72, pp. 4847–4854, 1950.

Manuscript received March 7, 2006 (e-mail: jeya@mail.kankyo.tohoku.ac.jp).

ADVANCED MATERIALS

DOI: 10.1002/adma.200601292

Chemical Synthesis of Sub-micrometer- to Nanometer-Sized Magnetic FeCo Dice**

By *Daisuke Kodama, Kozo Shinoda, Kimitaka Sato, Yoshihiro Konno, Raphael J. Joseyphus, Kenichi Motomiya, Hideyuki Takahashi, Takatoshi Matsumoto, Yoshinori Sato, Kazuyuki Tohji*, and *Balachandran Jeyadevan**

The synthesis of nanoparticles of, for example, Fe, Co, FePt, CoPt, or FeCo with enhanced magnetic properties is demanded for various applications in nano- and biotechnology.[1–5] Although a large number of reports have appeared in the recent past, most of the chemical synthesis techniques reported until now employ environmentally unfriendly chemicals and tedious synthesis processes that extend over a couple of days.[3,6] Especially in the case of FeCo, most of the techniques require high temperatures during synthesis as well as post-annealing treatments, and the potential to control the composition and purity[7,8] is not discussed in detail. The bulk FeCo alloy is used in various engineering applications because of its high saturation magnetization, high Curie temperature, high permeability, low coercivity, and anisotropy.[9] On the other hand, the potential of FeCo nanoparticles in various fields[10,11] has been envisaged but is yet to be fully explored due to their unavailability. Although there have been reports attempting the synthesis of FeCo bimetallic alloy particles by the polyol process[12] and by reduction of the metal ions with hydrazine hydrate in alcohol,[13] the composition could not be freely manipulated in both cases and the maximum concentration of Fe in FeCo particles was about 20 at %. Furthermore, the formation of alloy particles was not confirmed beyond doubt. Recently, attempts utilizing thermal decomposition techniques have resulted in the formation of FeCo particles, and the control over the stability[7] and purity[8] of the product has been achieved only through stringent steps during and after synthesis. However, the potential of these techniques for controlling the composition, size, shape, and other parameters that play an important role in defining the properties of the particles as well as their use in practical applications are neither discussed nor demonstrated. Thus, there is an urgent need for the development of a chemical synthesis technique that could overcome the above-mentioned drawbacks and form a basis for the synthesis of various alloy nanoparticles. Here, we report a simple technique to synthesize composition- and size-controlled cubic FeCo particles, ranging in size from a few hundred to tens of nanometers, at 403 K within one hour using a modified polyol process.

In the polyol process, the metal salts are dissolved in liquid polyol under an inert atmosphere and heated to elevated temperatures to obtain fine metal or alloy nanoparticles.[14] A typical experimental procedure to synthesize FeCo particles is as follows: FeCo alloy particles with varying chemical composition were prepared by using $FeCl_2 \cdot 4H_2O$, $Co(Ac)_2 \cdot 4H_2O$, and NaOH in ethylene glycol (EG). This solution was heated to the boiling point of EG, refluxed at this temperature for 1 h in the presence of a surfactant, and cooled to room temperature. The black precipitate obtained was recovered from the polyol, and washed and stored in ethanol. The total concentration of the metal salts was fixed at 0.01 mol L^{-1}, while the Fe/Co molar ratio was varied depending on the target alloy composition. The reduction of the metal hydroxides to their respective metals takes place through dehydration and oxidation reactions in EG;[15] however, the process may follow different paths, for example, reduction from hydroxides or oxides or the formation of metal complexes, depending on the types of metal salts and polyols. It should be remembered that the reaction rate (r) of the polyol process dictates the properties of the nanoparticles, such as composition (in the case of alloys), size, size distribution, crystal structure, and others, and is a function of various experimental parameters described by

$$r = f(P_{redox}, [M], [OH^-], T_{reac.}) \quad (1)$$

where P_{redox} is the reduction potential of the polyol, [M] is the metal-ion concentration, $[OH^-]$ is the concentration of hydroxyl ions, and $T_{reac.}$ is the reaction temperature.

[*] Prof. B. Jeyadevan, D. Kodama, Dr. K. Shinoda, Y. Konno, Dr. R. J. Joseyphus, K. Motomiya, Dr. H. Takahashi, Dr. T. Matsumoto, Dr. Y. Sato, Prof. K. Tohji
Graduate School of Environmental Studies
Tohoku University
Sendai 980-8579 (Japan)
E-mail: jeya@mail.kankyo.tohoku.ac.jp
K. Sato
Dowa Mining Company
Chiyoda-ku, Gaikanda, 4-14-1 Akihabara UDX Building
Tokyo 101-8671 (Japan)

[**] This work was supported by Grant-in-Aid for Basic Research #(A) 17201021 and #(S) 14103016 from the Ministry of Education, Science, Culture and Sport of Japan, and Grant-in-Aid # 0171078-A from the Iketani Science and Technology Foundation. We thank Dr. M. Doi and Prof. Y. Shimada, Tohoku University, for Mössbauer and high frequency measurements and Prof. A. Narayanasamy, University of Madras, for useful discussion and suggestions during the preparation of this manuscript. Supporting Information is available online from Wiley InterScience or from the author.

There are two possible routes through which one could succeed in the synthesis of alloy nanoparticles.[15] In the first route, the alloys are formed when the oxidation–reduction potentials of the metals are comparable, for example, Ni and Co. The inability of the reducing agent to reduce the metal ions together would result in the formation of separate metal entities, core/shell-structured composites or alloys, or in the reduction of one of the two metals. It should be noted that this argument is valid only when both the metal ions prevail in their reducible forms in solution. For example, the synthesis of metallic Co in EG is achieved with relative ease in the case of cobalt acetate, but not with cobalt chloride under similar experimental conditions. In the second route, the alloys are formed when one metal, which is easily reduced, acts as a catalyst and assists the reduction of the other, which is hard to reduce alone. Such a situation prevails in the case of noble-metal-based alloys such as FePt or CoPt.[4,16] Although the synthesis of magnetic transition-metal particles, such as Co and Ni, and noble-metal-based alloy particles has been comparatively straightforward, the formation of transition-metal alloys such as FeCo and FeNi is still a challenge. Thus, the synthesis of FeCo particles was attempted by controlling the parameters given in Equation 1 to facilitate the co-reduction of Fe and Co. Synthesis conditions in the conventional polyol process are unfavorable and led to the formation of additional phases such as α-Co and ferrite along with FeCo particles. To avoid the formation of multiple phases, precautionary measures, such as purging the system with inert gas, controlling the heating rate (to avoid the system remaining at any fixed temperature for an extended period of time), reaction temperature, and other parameters, were considered in modifying the process.

Although the proposed scheme has an edge over hitherto reported chemical techniques in obtaining pure FeCo particles, its potential could only be appreciated if control over the composition, size, size distribution, and shape of the alloy is accomplished. Previously, we reported the synthesis of Co metal particles with different sizes and crystal structures using the polyol process at temperatures below the boiling point of polyol.[17] On the contrary, Fe particles are formed in reasonable yield at temperatures as low as 393 K, while the formation of Co is not feasible. However, it should be noted that control over the reduction temperature could be obtained by varying $[OH^-]$.[18] Thus, both the reduction temperature and $[OH^-]$ become critical in the synthesis of alloys. Conditions outside the optimum values will result in alloys that are rich in either metal. In the case of FeCo, the particles became rich in Fe at lower reduction temperatures, whereas this was reversed at higher reduction temperatures. This is believed to be due to the intermediate compounds formed by Fe and Co as well as their stabilities against temperature. The presence of hydroxyl ions in the metal-ion–polyol system may act as a catalyst for accelerating the formation of precursor complexes.[19] Similar behavior has been observed in the case of Fe-particle synthesis in polyol,[20] where the polyol molecules were found to play a role in the reduction of Fe, and the yield as well as the particle size of Fe obtained depended on the type of polyol: When highly reducing 1,3-propanediol was used, the obtained particles were smaller in size compared to the EG case. Consequently, Fe particles of smaller size got oxidized comparatively easily, and the formation of magnetic iron oxide was also recorded besides the presence of the diffraction peak corresponding to Fe. Furthermore, the presence of hydroxyl ions in the system lowered the potential barrier and facilitated the formation of Fe in polyols at 393 K. Thus, under optimum experimental conditions, that is, optimum type of polyol and $[OH^-]$, oxide-phase-free Fe particles of a few hundred nanometers with a saturation magnetization value of 182 $A\,m^2\,kg^{-1}$ were realized.[20] These results proved that the formation of Fe particles in polyol is not due to the disproportionation reaction, where the presence of equal amounts of Fe and magnetite is a must. The authors are of the opinion that the Fe compound or complex formed at lower temperatures in the presence of hydroxyl ions requires less potential to form zero-valent Fe than that required of Co complexes. However, the presence of Fe, which acts as a catalyst, facilitates the reduction of Co at lower temperatures and leads to the formation of the FeCo alloy. On the other hand, the reduction of Co is very much enhanced at elevated temperatures compared to Fe, leading to Co-rich FeCo alloys irrespective of the initial Fe/Co ratio. It should be noted that at low temperatures, the Fe/Co composition could be easily controlled.

The FeCo particles with varying Fe concentrations (samples 1 to 6) were synthesized by reacting a specified ratio of Fe and Co salts of 0.01 $mol\,L^{-1}$ in EG at 403 K for 1 h. The hydroxyl-ion/metal molar ratio is fixed at 40:1. The X-ray diffraction (XRD) analysis of the particles obtained under varying molar concentrations of Fe (Fig. 1) recorded a pattern very similar to that of either Fe or FeCo and was free of any

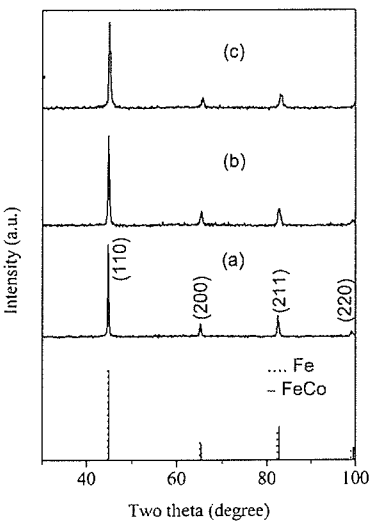

Figure 1. The XRD patterns of a) $Fe_{68}Co_{32}$, b) $Fe_{48}Co_{52}$, and c) $Fe_{25}Co_{75}$ synthesized at 403 K. The Fe and FeCo peak positions are represented at the bottom portion of the figure.

secondary phases. However, a slight variation in the peak position could be observed, especially the (220) peak, to higher angles on decreasing the initial molar concentration of Fe from 70 to 30 mol%. The analysis of the XRD data, using least-squares peak fitting, showed a lattice parameter variation of 2.8632 to 2.8460 Å within an error of ±0.0015 Å for the above samples. This variation is understandable because of the substitution of Co for Fe in α-Fe, the lattice parameter of which is 2.8665 Å, and agrees well with that of FeCo bulk. Moreover, to confirm the formation of FeCo, the samples were further analyzed using extended X-ray absorption fine structure (EXAFS) spectroscopy. Although the EXAFS spectra of the alloys are similar across the entire composition range, a representative result of the $Fe_{68}Co_{32}$ alloy is presented here.

The EXAFS spectra of the FeCo particles at the Fe K (7111 eV) and Co K (7709 eV) absorption edges confirmed the presence of both metals and showed a strong resemblance to each other, as shown in Figure 2. Furthermore, no peaks corresponding to the presence of any metal oxides were observed in the X-ray absorption near-edge spectroscopy (XANES) region at both absorption edges. The Fourier transforms (FTs) of the k^3-weighted EXAFS spectra (see Supporting Information, Fig. S1) measured at the Fe and Co K-edges are given in Figure 3a–d. The FT spectra of Co (Fig. 3c) in the FeCo particles is similar to that of Fe in α-Fe (Fig. 3b) rather than α-Co (Fig. 3d). Further analysis of fine-structural details from the FT spectra is not possible because the backscattering amplitude and phase shift of Fe and Co are very similar (Fig. S2). Furthermore, if we assume a body-centered cubic (bcc) structure, the FT profile fits very well with two shells having interatomic distances of 0.248 and 0.287 nm. Assuming the Co occupies the body center and the Fe occupies the corners, or assuming the Co occupies both the body center and the corners, the FT profile fits very well. Also, a similar fitting that assumed an α-Co structure with a single shell having an atomic distance of 0.249 nm was poor. The above structural analysis suggests that the FeCo particles consist of an Fe bcc lattice, where Fe atoms are partly replaced by Co. The formation of either a Co shell and an Fe core or vice versa is also ruled out by the above analysis.

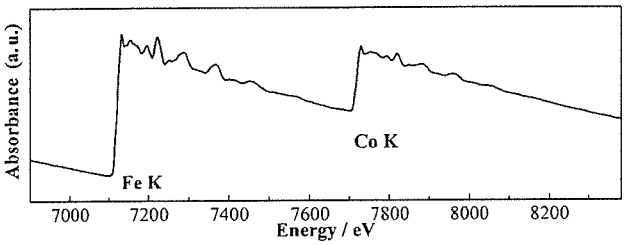

Figure 2. Raw EXAFS spectra of $Fe_{68}Co_{32}$ particles at the Fe and Co K absorption edges.

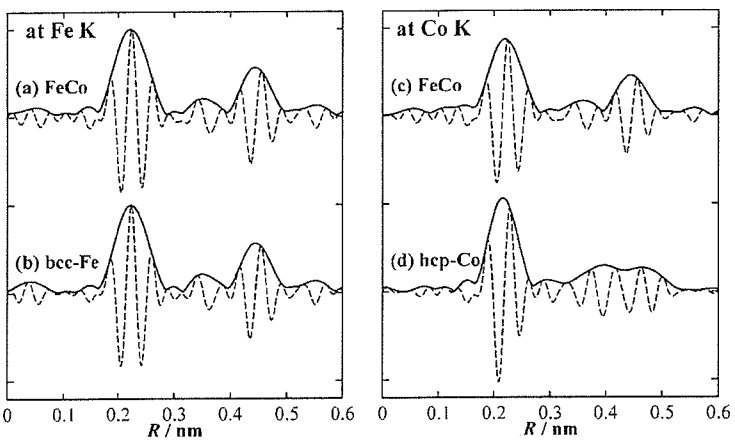

Figure 3. The FT spectra of a) $Fe_{68}Co_{32}$ and b) α-Fe foil at the Fe K-edge, and c) $Fe_{68}Co_{32}$ and d) α-Co at the Co K-edge.

X-ray fluorescence (XRF) analysis was carried out to determine the final composition of the powders within an estimated error of 5%. The final compositions of samples 1 to 6 were very close to the initial molar concentrations of Fe and Co, as given in Table 1. The compositional analysis of the particles by transmission electron microscopy energy dispersive X-ray (TEM-EDX) spectroscopy was within the error limits of the XRF data.

FeCo alloys in the Fe composition range 70–30 at% undergo an order–disorder transition at around 1000 K, in which the structure changes between disordered bcc (α) to ordered B2 (CsCl, or α′) type. The ordered–disordered nature of the FeCo samples is not known for the chemically prepared samples as most of the synthesis techniques for the FeCo alloys are undertaken at high temperatures. A representative result for the $Fe_{68}Co_{32}$ alloy showed that the low-temperature order–disorder transition takes place at around 875–945 K, followed by the face-centered cubic (fcc) (γ) phase transition at 1259 K, and melting at 1766 K (Fig. S3); these transition temperatures are close to those of the bulk.[21] Also, Mössbauer spectroscopy was employed to study the ordered or disordered nature of the samples. The hyperfine field of the ordered FeCo was found to be lower than the disordered FeCo, with the maximum decrease at the equiatomic composition.[22] Room-temperature Mössbauer spectra of the FeCo alloy samples in the Fe molar range from 90 to 20 mol% were measured, and the Mössbauer parameters (isomer shift and hyperfine field) are shown in Figure 4. The Mössbauer spectrum is fitted with a single sextet and a superparamagnetic component of Fe, and its oxides were not present in any of the samples (Fig. S4). The hyperfine field increases with decreasing molar Fe concentration up to 60 at% and then decreases. It has been reported that the maximum hyperfine field of 36.5 T occurs at 25 at% Co for disordered FeCo.[22] In the present case, the maximum may lie between 70 and 60 at% Fe and decreases thereafter. As the hyperfine field of ordered $Fe_{50}Co_{50}$ is reported to be around 35.0 T,[20]

Table 1. The initial FeCo composition [at%] and the final composition [at%] obtained for the FeCo alloy synthesized at 403 K.

Sample	Initial FeCo	Final composition
1	$Fe_{90}Co_{10}$	$Fe_{85}Co_{15}$
2	$Fe_{80}Co_{20}$	$Fe_{77}Co_{23}$
3	$Fe_{70}Co_{30}$	$Fe_{68}Co_{32}$
4	$Fe_{60}Co_{40}$	$Fe_{62}Co_{38}$
5	$Fe_{50}Co_{50}$	$Fe_{48}Co_{52}$
6	$Fe_{30}Co_{70}$	$Fe_{25}Co_{75}$

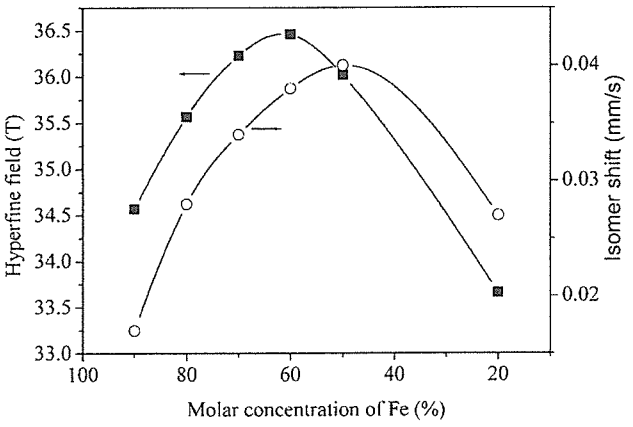

Figure 4. Mössbauer parameters (isomer shift and hyperfine field) of the FeCo alloy for various molar concentrations of Fe.

the higher hyperfine field of 36.0 T for the $Fe_{48}Co_{52}$ for an Fe molar concentration of 50 at% suggests that the ordering is less pronounced in the chemically synthesized samples. The local environment of the Fe atoms in such disordered solids also influences the hyperfine fields, and hence deviations in maximum values are observed compared to the bulk FeCo. The isomer-shift values increase with the molar concentration of Fe and are expected to show a maximum at 75 at% Fe.[23] However, we observed a continuous increase up to 50 at%, suggesting that the disorder present in the system has altered the d-electron density. Detailed analysis on the order–disorder phenomena is in progress.

The shape of the FeCo particles varied from cubic to nearly spherical when the particles were rich in Fe or Co, respectively. It has been reported that the cubic shape of gold and silver particles is influenced by the selective absorption of poly(vinyl pyrrolidine) (PVP) on various crystallographic planes.[24] In our system the Fe-rich FeCo particles assume a cubic shape while Co-rich particles assume a nearly spherical shape, irrespective of the presence of PVP. However, it should be noted that the degree of agglomeration is reduced in the presence of PVP during the synthesis. When the FeCo particles are rich in Fe, they crystallize to the bcc structure and the morphology is governed by the stable crystal plane (110), which leads to the formation of cubic structures as in the case of pure iron.[25] Generally, the size of the particles can be controlled by the parameters described in Equation 1. When the P_{redox} of the polyol is high, the size of the particles becomes smaller, provided that the rest of the conditions remain constant. Here, the metal ions are reduced rapidly, forming an avalanche of nuclei that consume a large portion of the metal species, and the particle diameter is consequently reduced due to the limited supply of metal ions left for growth. The reaction rate could also be enhanced by either increasing [M] or raising the temperature ($T_{reac.}$). Furthermore, the reaction rate is enhanced when [OH^-] in the metal-ion–polyol system is increased. The concentration of hydroxyl ions required for maintaining a specific rate depends on the type of polyol. Highly reducing polyols need smaller amounts of hydroxyl ions to synthesize particles of comparable diameters. In the present system, the number of nuclei formed is strongly dependent on [OH^-], and the excess metal ions present in the solution are utilized for the growth of these nuclei. Thus, the size of the particles was tuned by controlling [M] while keeping [OH^-] and the Fe/Co metal ratio constant. The particle size decreased from 300 to 35 nm for the $Fe_{68}Co_{32}$ alloy with a decrease in metal-ion concentration from 0.07 to 0.015 mol L^{-1}, as shown in Figure 5a–c. Although agglomeration of the particles was evidenced in most of the samples, isolated particles could also be obtained, as shown in Figure 5c. Further work is in progress to obtain colloidal dispersions of particles using surfactants such as oleic acid and oleylamine, as in the case of other alloys.[26] The lowest particle size of 35 nm in the present study enables ferromagnetic behavior as evidenced from the Mössbauer studies, whereas the superparamagnetic size limit of the alloy, found by substituting the value of anisotropy constant, K for FeCo[27] in Equation 2, is around 6 nm.

$$V = \frac{k_B T \ln(\tau_m/\tau_0)}{K} \quad (2)$$

Here V is the volume of the particle, k_B is the Boltzmann constant, T is the temperature, which is taken as 300 K, and τ_m and τ_0 are the measured relaxation time and the relaxation time constant, the values of which are 10^{-8} and 10^{-13} s, respectively.

The saturation magnetization of the FeCo alloy is known to vary depending on the concentration of Fe in the particles,

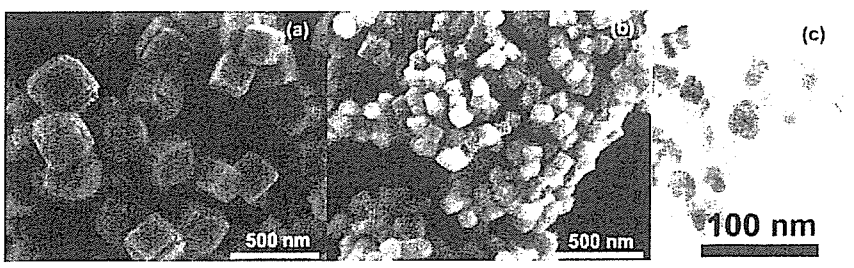

Figure 5. Particle size variation of the $Fe_{68}Co_{32}$ alloy synthesized with metal-ion concentrations of a) 0.07 b) 0.03, and c) 0.015 mol L^{-1}.

ADVANCED MATERIALS

showing a maximum of around 240 $A\,m^2\,kg^{-1}$ close to an Fe/Co ratio of two.[28] The saturation magnetization of the FeCo particles measured using a maximum applied field of 1.5 T recorded a maximum value of 225 $A\,m^2\,kg^{-1}$ for the $Fe_{68}Co_{32}$ alloy (composition determined from XRF analysis), as shown in Figure 6. In other cases, the saturation magnetization value lay between 200 and 210 $A\,m^2\,kg^{-1}$. The high magnetization value in $Fe_{68}Co_{32}$ is greater than that of the bulk Fe, which is also an indication of the formation of the alloy. Apart from the composition,[29] the variations in the saturation magnetization of these alloys could also be attributed to the ordered–disordered nature of these alloys.

Although the stability of the particles was demonstrated with no additional care being taken during handling for all the above measurements, the long-term stability of the particles is desired from an application point of view. The magnetic hysteresis loops of the samples after subjection to a temperature of 333 K and 90 % humidity for seven days decreased by only 20 %; comparable to particles used in any practical application. The potential of these particles in high-frequency applications is being investigated, and the results of the preliminary measurements have recorded resonance properties reflecting the monodispersity of the samples (Fig. S5). In addition, this work can be extended to obtain colloidal dispersed crystals coated with suitable biocompatible surface modifiers for proposed medical diagnostics and therapies,[30,31] which will foster innovative fields of medicine.

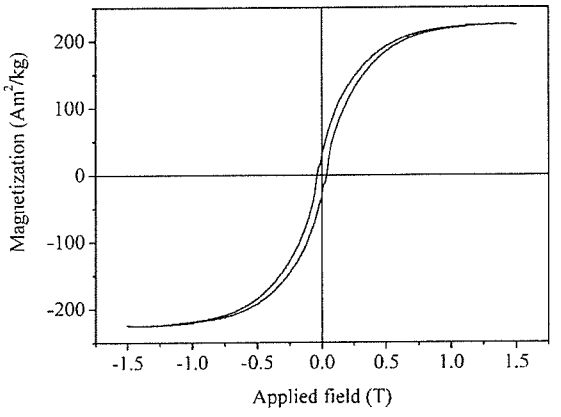

Figure 6. The hysteresis loop of the $Fe_{68}Co_{32}$ alloy showing maximum magnetization at 300 K.

Experimental

FeCo alloy particles with varying chemical composition and sizes were prepared by using $FeCl_2 \cdot 4\,H_2O$, $Co(Ac)_2 \cdot 4\,H_2O$ (Ac: acetate), and NaOH in ethylene glycol (EG). The EG/metal salts/NaOH system was heated to the required temperature, refluxed for 1 h in the presence of PVP, and cooled to room temperature. The black precipitate thus obtained was recovered from polyol and washed and stored in ethanol. The FeCo particles with varying Fe content (samples 1 to 6) were synthesized by reacting specified ratios of Fe and Co salts of 0.01 $mol\,L^{-1}$ in EG at 403 K for 1 h. The OH^-/metal molar ratio was fixed at 40:1. The size of the particles was tuned by controlling [M] from 0.07 to 0.015 $mol\,L^{-1}$ while keeping [OH^-] and the Fe/Co metal ratio constant.

Characterization: Powder XRD data was recorded at room temperature in a Rigaku X-ray diffractometer using a Cu target. Scanning electron microscopy (SEM) and high-resolution transmission electron microscopy (HRTEM) measurements were undertaken using Hitachi S-4100 and HF-2000 electron microscopes, respectively. X-ray fluorescent measurements of the samples were conducted in a Horiba MESA-500W instrument. The EXAFS measurements were performed in a Rigaku spectrometer. Thermal measurements were undertaken using a Bruker DSC 3300 high-temperature differential scanning calorimeter. Mössbauer measurements were recorded for the samples of various compositions at room temperature using a Wissel Mössbauer spectrometer calibrated with Fe. The isomer-shift values are reported with respect to α-Fe at room temperature. Magnetic measurements at room temperature were conducted using a Tamakawa VSM up to a maximum field of 1.5 T calibrated with standard Ni.

Received: June 12, 2006
Revised: August 14, 2006

[1] S. Yamamuro, T. Ando, K. Sumiyama, T. Uchida, I. Kojima, *Jpn. J. Appl. Phys.* **2004**, *43*, 4458.
[2] V. F. Puntes, K. M. Krishnan, A. P. Alivisatos, *Science* **2001**, *291*, 2115.
[3] S. H. Sun, C. B. Murray, D. Weller, L. Folks, A. Moser, *Science* **2000**, *287*, 1989.
[4] C. N. Chinnasamy, B. Jeyadevan, K. Shinoda, K. Tohji, *J. Appl. Phys.* **2003**, *93*, 7583.
[5] G. Ennas, A. Falqui, S. Marras, C. Sangregorio, G. Marongiu, *Chem. Mater.* **2004**, *16*, 5659.
[6] T. Hyeon, S. S. Lee, J. Park, Y. Chung, N. H. Bin, *J. Am. Chem. Soc.* **2001**, *123*, 12798.
[7] H. Bonnemann, R. A. Brand, W. Brijoux, H. W. Hofstadt, M. Frerichs, V. Kempter, W. M. Friedrichs, N. Matoussevitch, K. S. Nagabhushana, F. Voigts, V. Caps, *Appl. Organomet. Chem.* **2005**, *19*, 790.
[8] C. Desvaux, C. Amiens, P. Fejes, P. Renaud, M. Respaud, P. Lecante, E. Snoeck, B. Chaudret, *Nat. Mater.* **2005**, *4*, 750.
[9] *Ferromagnetic Materials* (Ed: E. P. Wohlfarth), North-Holland, Amsterdam **1980**.
[10] N. H. Duc, T. M. Danh, N. A. Tuan, J. Teillet, *Appl. Phys. Lett.* **2001**, *78*, 3648.
[11] R. S. Sundar, S. C. Deevi, *Int. Mater. Rev.* **2005**, *50*, 157.
[12] G. Viau, F. Fievet-Vincent, F. Fievet, *J. Mater. Chem.* **1996**, *6*, 1047.
[13] X. Su, H. Zheng, Z. Yang, Y. Zhu, A. Pan, *J. Mat. Sci.* **2003**, *38*, 4581.
[14] F. Fievet, J. P. Lagier, B. Blin, B. Beaudoin, M. Figlarz, *Solid State Ionics* **1989**, *32*, 198.
[15] D. Larcher, R. Patrice, *J. Sol. State Chem.* **2000**, *154*, 405.
[16] B. Jeyadevan, K. Urakawa, A. Hobo, N. Chinnasamy, K. Shinoda, D. D. J. Djayaprawira, M. Tsunoda, M. Takahashi, *Jpn. J. Appl. Phys.* **2003**, *42*, L350.
[17] O. Perales-Perez, B. Jeyadevan, C. N. Chinnasamy, K. Tohji, A. Kasuya, in *Recent Advances in Inorganic Materials* (Eds: D. Bahadur, S. Vitta, O. Prakash), Narosha Publishing House, New Delhi, **2004**.
[18] R. J. Joseyphus, B. Jeyadevan, K. Shinoda, Y. Sato, K. Tohji, presented at *Proc. ISHR & ICSTR 2006*, Sendai, Japan, August 5–9 **2006**.
[19] B. Jeyadevan, K. Shinoda, R. J. Justin, T. Matsumoto, K. Sato, H. Takahashi, Y. Sato, K. Tohji, *IEEE Trans. Magn.* **2006**, *42*, 3030.
[20] R. J. Joseyphus, D. Kodama, T. Matsumoto, B. Jeyadevan, Y. Sato, K. Tohji, presented at *Proc. ICM 2006*, Kyoto, Japan, August 20–25 **2006**.
[21] R. M. Bozorth, *Ferromagnetism*, D. Van Nostrand Co. Inc., New York, **1951**, Ch. 2.
[22] B. deMayo, D. W. Forester, S. Spooner, *J. Appl. Phys.* **1970**, *41*, 1319.

[23] H. H. Hamdeh, B. Fultz, D. H. Pearson, *Phys. Rev. B: Condens. Matter Mater. Phys.* **1989**, *39*, 11 233.
[24] Y. Sun, Y. Xia, *Science* **2002**, *298*, 2176.
[25] F. Dumestre, B. Chaudret, C. Amiens, P. Renaud, P. Fejes, *Science* **2004**, *303*, 821.
[26] Y. Sasaki, M. Mizuno, A. C. C. Yu, T. Miyauchi, D. Hasegawa, T. Ogawa, M. Takahashi, B. Jeyadevan, K. Tohji, K. Sato, S. Hisano, *IEEE Trans. Magn.* **2005**, *41*, 660.
[27] J. W. Shih, *Phys. Rev.* **1934**, *46*, 139
[28] P. Weiss, R. Forrer, *Ann. Phys.* **1929**, *12*, 279.
[29] D. I. Bardos, *J. Appl. Phys.* **1969**, *40*, 1371.
[30] G. Reiss, A. Hutten, *Nat. Mater.* **2005**, *4*, 725.
[31] A. Hutten, D. Sudfeld, I. Ennen, G. Reiss, W. Hachmann, U. Heinzmann, K. Wojczykowski, P. Jutzi, W. Saikaly, G. Thomas, *J. Biotech.* **2004**, *112*, 47.

Available online at www.sciencedirect.com
SCIENCE DIRECT
Thin Solid Films 506–507 (2006) 259 – 262
www.elsevier.com/locate/tsf

Effects of strong magnetic field on carbon nanotube formation using rf glow-discharge plasma

T. Kaneko [a,*], H. Matsuoka [a], T. Hirata [a], R. Hatakeyama [a], K. Tohji [b]

[a] *Department of Electronic Engineering, Tohoku University, Sendai 980-8579, Japan*
[b] *Graduate School of Environmental Studies, Tohoku University, Sendai 980-8579, Japan*

Available online 19 September 2005

Abstract

We have investigated the formation of uniform and well-aligned multi-walled carbon nanotubes (MWNTs) by controlling radio-frequency (rf) glow-discharge plasmas in weak and strong magnetic fields. The MWNTs growing directly on the rf electrode in the weak magnetic field (0.03 T) are deformed and combined with each other by the bombardment of the high energy ions generated by the large sheath electric field in front of the rf electrode. When the strong magnetic field (2 T) is applied, on the other hand, the MWNTs are observed to be well-aligned and not to be deformed. These results can be explained by the fact that the ion bombardment energy reduces in spite of the existence of the large sheath electric field, which is caused by the magnetization of the ions in the strong magnetic field.

Keywords: Carbon nanotubes; Plasma-enhanced chemical vapor deposition; Strong magnetic field; Ion bombardment energy

1. Introduction

Carbon nanotubes well-aligned perpendicularly to substrates have been claimed for a variety of applications such as nanoelectronic devices, field emitters, and scanning probes, and the formation of these nanotubes has been developed by various methods such as chemical vapor deposition (CVD) [1], hot-filament CVD [2], and plasma-enhanced CVD (PECVD) [3]. Recently, the production of uniform and well-aligned carbon nanotubes by the PECVD using a magnetron type radio-frequency (rf) glow-discharge plasma has been performed [4–7], and it has been demonstrated that the nanotubes are effectively produced on a cylindrical rf electrode which is negatively self-biased and exposed to a strong plasma-sheath voltage drop. However, the strong sheath voltage generates the high energy ions which impinge on the rf electrode, resulting in the deformation of the nanotubes well-aligned on the rf electrode [7]. Thus, in order to prevent the high energy ions from directly impinging on the rf electrode, i.e., the nanotubes, we introduce strong magnetic fields which are externally applied with a superconducting magnet in a way that the field lines are perpendicular to the plasma-sheath electric field. Although the synthesis of carbon nanotubes in the strong magnetic field up to 10 Tesla (T) has been performed using an arc discharge plasma [8], almost no experimental results have been reported concerning plasma diagnostics, and the effects of the strong magnetic field on the plasma parameter and resultant nanotube growth have not yet been clarified.

In this paper, we characterize the plasma parameter under the strong magnetic field condition and clarify phenomena associated with nanotube growth and plasma effect.

2. Experimental apparatus

The schematic of an experimental apparatus is shown in Fig. 1. A magnetron type rf (13.56 MHz) glow-discharge plasma is generated, where a powered cylindrical rf electrode (25 mm in diameter) is made of Ni and installed in the center of a grounded cylindrical chamber (84 mm in diameter and 600 mm in length). In order to control the plasma parameter including the sheath voltage, a strong

* Corresponding author.
E-mail address: kaneko@ecei.tohoku.ac.jp (T. Kaneko).

0040-6090/$ - see front matter © 2005 Elsevier B.V. All rights reserved.
doi:10.1016/j.tsf.2005.08.164

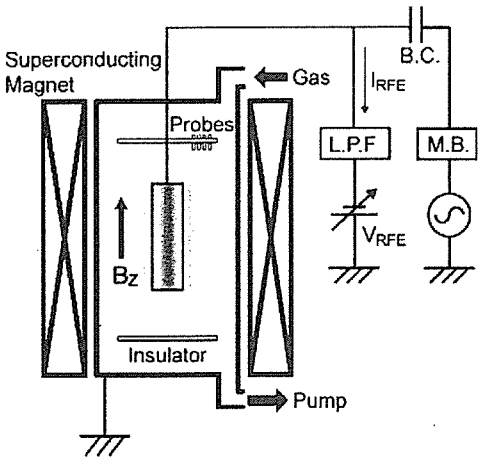

Fig. 1. Schematic of experimental apparatus.

magnetic field is externally imposed parallel to a powered rf electrode, i.e., perpendicularly to the sheath electric field, using a Gifford–McMahon (GM) cryocooled superconducting magnet with a 400-mm-diameter and 505-mm-length magnet bore which produces the strong magnetic field of 4 T (max) at the axis center of the bore. The glow-discharge is driven by a rf power source through a matching box (M.B.) and a blocking capacitor (B.C.). The plasma system for the nanotube growth is operated at the rf power of 1400 W, and dc bias voltage component (V_{RFE}) of and dc current density (I_{RFE}) toward the rf electrode can be externally controlled by connecting a dc power supply through a low-pass filter (L.P.F) circuit. In addition, the geometrically unique point different from the prevailing PECVD unit is that the active rf electrode with a cylindrical shape plays both the catalytic and deposite-substrate role. As a hydrocarbon source and dilution gas for the nanotube growth, methane (CH_4) and hydrogen (H_2) are used, respectively, with a mixture ratio of $CH_4:H_2=9:1$ at a total gas pressure of 0.1 Torr. The plasma density n_e, electron temperature T_e, and plasma potential ϕ_s are measured by a Langmuir probe and time varying and averaged current–voltage characteristics are carefully analyzed.

3. Results and discussion

In order to clarify the plasma characteristics in the strong magnetic field up to 2 T, argon gas is used here for generating the plasma because the methane plasma immediately contaminates the probe and interferes with the accurate measurements. Furthermore, the measurement of plasma parameter is performed at the low rf power of 600 W for protection of the probe measurement system.

Fig. 2(a) shows dependences of dc self-bias voltage of the rf electrode V_{RFE} and plasma potential ϕ_s on magnetic field B_z. The rf electrode is not connected to the dc power supply, i.e., the potential of the rf electrode is floating. When the magnetic field is changed to increase with the rf electrode kept at floating potential, V_{RFE} gradually increases and changes to the positive value for $B_z>0.4$ T. On the other hand, ϕ_s is positive in the weak magnetic field ($B_z=0.03$ T) and gradually changes to negative value with an increase in B_z. Here, the sheath voltage is defined as $V_{sh}=V_{RFE}-\phi_s$, which can evaluate the sheath electric field in front of the rf electrode. The strong magnetic field is found to change V_{sh} from negative ($V_{sh}=-130$ V at $B_z=0.03$ T) to positive ($V_{sh}=+40$ V at $B_z=2$ T), namely from the ion sheath to the electron sheath. Based on the result of the sheath voltage, it is expected that the ions which impinge on the rf electrode can be accelerated by the ion sheath and have high energy (>100 eV) at $B_z=0.03$ T, while the ions gradually decelerated and ultimately reflected by the electron sheath for the stronger magnetic field. Here, it is confirmed that the plasma density increases with an increase in the magnetic field due to the improved confinement by magnetron effect, but is almost constant ($\sim 10^{11}$ cm^{-3}) for $B_z>0.4$ T.

Fig. 2(b) presents dependences of dc bias voltage of the rf electrode V_{RFE} and plasma potential ϕ_s on the magnetic field B_z, where V_{RFE} is fixed at -110 V which corresponds to the floating potential of the rf electrode at $B_z=0.03$ T. Although ϕ_s is found to decrease with an increase in B_z in the same way as the case that the rf electrode is floating, the sheath voltage is always negative. The absolute value of the sheath voltage $|V_{sh}|$ reduces for the stronger magnetic field, however $|V_{sh}|$ remains enough large (>40 V) at $B_z=2$ T. Here, the ion energy impinging on the rf electrode is calculated in consideration of the effect of the magnetic field applied perpendicularly to the sheath electric field. An ion drift velocity v_{di} which

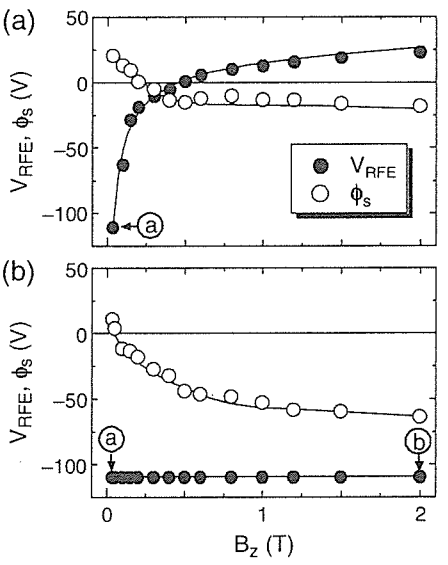

Fig. 2. Dependences of dc bias voltage of the rf electrode V_{RFE} and plasma potential ϕ_s on magnetic field B_z. The rf electrode is (a) electrically floating and (b) biased at $V_{RFE}=-110$ V.